Fusion, fission, and transport control asymmetric inheritance of mitochondria and protein aggregates

Stefan Böckler,[1]* Xenia Chelius,[1]* Nadine Hock,[1]* Till Klecker,[1] Madita Wolter,[1] Matthias Weiss,[2] Ralf J. Braun,[1] and Benedikt Westermann[1]

[1]Zellbiologie and [2]Experimentalphysik I, Universität Bayreuth, Bayreuth, Germany

Partitioning of cell organelles and cytoplasmic components determines the fate of daughter cells upon asymmetric division. We studied the role of mitochondria in this process using budding yeast as a model. Anterograde mitochondrial transport is mediated by the myosin motor, Myo2. A genetic screen revealed an unexpected interaction of *MYO2* and genes required for mitochondrial fusion. Genetic analyses, live-cell microscopy, and simulations in silico showed that fused mitochondria become critical for inheritance and transport across the bud neck in *myo2* mutants. Similarly, fused mitochondria are essential for retention in the mother when bud-directed transport is enforced. Inheritance of a less than critical mitochondrial quantity causes a severe decline of replicative life span of daughter cells. Myo2-dependent mitochondrial distribution also is critical for the capture of heat stress–induced cytosolic protein aggregates and their retention in the mother cell. Together, these data suggest that coordination of mitochondrial transport, fusion, and fission is critical for asymmetric division and rejuvenation of daughter cells.

Introduction

During the cell cycle, membrane-bounded organelles must grow, multiply, and travel to their proper positions in the daughter cells. Depending on the organelle and cell type, ordered or stochastic strategies ensure faithful organelle inheritance (Warren and Wickner, 1996). In asymmetrically dividing cells, organelles are frequently partitioned in a specialized manner to produce daughter cells with distinct fates. This generates cellular diversity and contributes to differentiation or maintenance of stem cell properties in metazoans or counterbalances aging in unicellular organisms (Ouellet and Barral, 2012). For example, stem cells selectively partition aged mitochondria to differentiating daughter cells, whereas apportioning of young organelles is required to maintain stemness properties (Katajisto et al., 2015). Similarly, damaged and dysfunctional cellular components and organelles are retained in yeast mother cells, whereas highly functional organelles are inherited to the bud (Henderson and Gottschling, 2008; Higuchi-Sanabria et al., 2014; Nyström and Liu, 2014).

Much progress in the study of organelle inheritance in asymmetrically dividing cells has been made with budding yeast, *Saccharomyces cerevisiae* (Pruyne et al., 2004; Ouellet and Barral, 2012; Westermann, 2014; Knoblach and Rachubinski, 2015). Mitochondria are transported along actin cables toward the bud by the class V myosin Myo2 (Altmann et al., 2008; Förtsch et al., 2011; Chernyakov et al., 2013). Anterograde Myo2-dependent transport is aided by a small rab-type GTPase, Ypt11 (Itoh et al., 2002; Lewandowska et al., 2013). Mmr1 is a mitochondria-associated protein that promotes mitochondrial inheritance either by supporting recruitment of Myo2 to mitochondria (Itoh et al., 2004; Eves et al., 2012; Chernyakov et al., 2013) or by anchoring newly inherited mitochondria to the bud tip (Swayne et al., 2011). At the same time, a portion of the mitochondrial network is retained in the mother cell by plasma membrane anchors containing Num1 and Mdm36 (Klecker et al., 2013; Lackner et al., 2013; Ping et al., 2016) or a mitochondrial F-box protein, Mfb1 (Pernice et al., 2016). Anterograde mitochondrial transport is balanced by retrograde mitochondrial movements by yet unknown mechanisms (Fehrenbacher et al., 2004). Thus, the machineries mediating anterograde and retrograde transport together with anchors at the bud tip and mother cell cortex coordinate proper partitioning of mitochondria in dividing yeast cells.

A yeast mother cell can produce only a limited number of daughter cells. Although each bud is born young, independent of the age of its mother, the mother cell grows older each generation and eventually dies (Mortimer and Johnston, 1959). This process is called replicative aging (Longo et al., 2012). Intriguingly, mechanisms exist to establish functional asymmetry between retained and inherited mitochondria. The quantity of mitochondria partitioned to the bud is precisely controlled, whereas the mitochondrial quantity retained in

*S. Böckler, X. Chelius, and N. Hock contributed equally to this paper.

Correspondence to Benedikt Westermann: benedikt.westermann@uni-bayreuth.de

Abbreviations used: 5-FOA, 5-fluoroorotic acid; GO, gene ontology; mtDNA, mitochondrial DNA; mtERFP, mitochondria-targeted enhanced RFP; mtGFP, mitochondria-targeted GFP; mtRFP, mitochondria-targeted RFP; SCD, synthetic complete dextrose medium; SGA, synthetic genetic array.

The Rockefeller University Press
J. Cell Biol. Vol. 216 No. 8 2481–2498
https://doi.org/10.1083/jcb.201611197

the mother declines with age (Rafelski et al., 2012). Furthermore, less functional and aged mitochondria are thought to be retained in mother cells, whereas buds receive highly functional organelles (McFaline-Figueroa et al., 2011; Hughes and Gottschling, 2012; Pernice et al., 2016). However, only little is known about the cellular pathways and molecular mechanisms that contribute to the partitioning of mitochondria between mother and daughter cells.

The accumulation of cytosolic protein aggregates in mother cells is another hallmark of aging yeast cells (Erjavec et al., 2007; Zhou et al., 2011; Nyström and Liu, 2014; Miller et al., 2015b). Three controversial models were suggested to explain how buds are kept free from protein aggregates. First, protein aggregates were proposed to bind to actin cables and move toward the mother cell by the retrograde flow of actin cables originating at the bud tip (Liu et al., 2010). Second, aggregated proteins were suggested to be sequestered in specialized compartments, termed INQ/JUNQ, CytoQ, and IPOD, that are attached to the nucleus or vacuole (Spokoini et al., 2012; Miller et al., 2015a; Hill et al., 2016). Third, protein aggregates were proposed to initially bind to the surface of the ER and then be transferred to mitochondria, thereby constraining their mobility and retaining them in the mother cell (Zhou et al., 2014). The contribution of these pathways to the retention of protein aggregates in the mother cell is a matter of ongoing debate (Liu et al., 2011; Nyström and Liu, 2014; Miller et al., 2015b).

In sum, it is thought that the machinery of mitochondrial inheritance contributes to the establishment of cellular asymmetry in three different ways. First, it controls the mitochondrial quantity apportioned to the growing bud (Rafelski et al., 2012). Second, through yet unknown mechanisms, it promotes the inheritance of highly functional mitochondria to the bud (McFaline-Figueroa et al., 2011; Hughes and Gottschling, 2012; Pernice et al., 2016). Third, it possibly also plays a role in the retention of damaged cytosolic proteins and aggregates in the mother cell (Zhou et al., 2014). Here, we identified mitochondrial fusion as a novel pathway contributing to Myo2-dependent transport of a critical mitochondrial quantity into the bud. Also, the replicative lifespan and retention of protein aggregates in the mother cell depend on the activity of the mitochondrial transport machinery. We conclude that the coordinated action of mitochondrial fusion/fission dynamics and transport determines mitochondrial inheritance and partitioning of cytosolic protein aggregates.

Results

Genetic interactions of *myo2* with genes of nuclear inheritance, mitochondrial distribution, and mitochondrial fusion pathways

Myo2 is a class V myosin motor powering bud-directed transport of membrane-bounded organelles, including secretory vesicles, peroxisomes, late Golgi, vacuoles, and mitochondria (Matsui, 2003; Altmann et al., 2008). Its C-terminal cargo-binding domain contains a proximal binding site for mitochondria and vacuoles and a distal binding site for secretory vesicles and peroxisomes (Pashkova et al., 2006; Altmann et al., 2008; Eves et al., 2012). The *myo2(LQ)* allele contains two amino acid substitutions, Q_{1233} to R and L_{1301} to P, in the mitochondria-binding site. The *myo2(LQ)* mutant has severe inheritance defects for mitochondria and vacuoles, whereas the transport of secretory vesicles, late Golgi, peroxisomes, and ER is not compromised. Mitochondria typically accumulate at the mother cell pole opposite of the bud, and only few mitochondria pass the bud neck and enter the daughter cell (Förtsch et al., 2011; Fig. 1 A).

To screen for genes interacting with *MYO2* we introduced the *myo2(LQ)* allele into the yeast deletion library (Giaever et al., 2002) by synthetic genetic array (SGA) technology (Baryshnikova et al., 2010). Two independent SGA screens with more than 4,000 double mutants in each round (Table S1) identified 94 gene deletions that reproducibly produced strong negative interactions (Table S2). Gene ontology (GO) terms indicate which genes are involved in similar cellular processes. GO terms analysis of negative *myo2(LQ)* interactors revealed an enrichment of genes related to nuclear inheritance and mitochondrial distribution (Fig. 1 B).

In addition to its role in organelle transport, Myo2 is required for positioning of the mitotic spindle by binding to microtubule plus ends through interaction with Kar9 and Bim1 (Hwang et al., 2003). As the L_{1301} residue in the Myo2 cargo-binding domain is critical for interaction with Kar9 (Eves et al., 2012), we expected to find genetic interactions with genes required for nuclear inheritance. Interestingly, *myo2(LQ)* shows a strong negative genetic interaction with Δ*num1* (Fig. 1, C and D). Num1 is a cell cortex–associated protein involved both in nuclear and mitochondrial partitioning (Farkasovsky and Küntzel, 1995; Klecker et al., 2013; Lackner et al., 2013). To test whether inheritance defects of mitochondria or nuclei cause the synthetic growth defect, we examined the distribution of mitochondria and nuclei in budding cells. Mitochondrial inheritance defects in *myo2(LQ)* Δ*num1* double mutants were very similar to *myo2(LQ)* single mutants, suggesting that there is no synthetic defect in mitochondrial transport (Fig. 1, E and F). Wild type cells and *myo2(LQ)* single mutants always contained a single nucleus per cell, whereas ∼11% of Δ*num1* cells contained more than one nucleus. This defect was markedly increased in *myo2(LQ)* Δ*num1* double mutants, which contained supernumerary nuclei in 26% of the cells (Fig. 1 G). This suggests that the negative genetic interactions of *myo2(LQ)* with Δ*num1* and other genes involved in nuclear inheritance reflect the function of Myo2 in mitotic spindle orientation.

The SGA screen also revealed several negative genetic interactions with genes known to be involved in mitochondrial distribution and inheritance, including *GEM1*, *MDM34*, *MMM1*, *PTC1*, and *YPT11*. All of these mutants are known to have defects in mitochondrial inheritance (Burgess et al., 1994; Roeder et al., 1998; Itoh et al., 2002; Frederick et al., 2004; Youngman et al., 2004) and, in the case of Δ*ypt11*, to be synthetic lethal with *myo2(LQ)* (Förtsch et al., 2011). These genes were expected to genetically interact with *myo2(LQ)* in an SGA analysis.

Intriguingly, two genes encoding core components of the mitochondrial fusion machinery, *FZO1* and *UGO1*, were found among the *myo2(LQ)* interactors. Mitochondrial fusion mutants are known to have fragmented mitochondria devoid of mitochondrial DNA (mtDNA; Hermann et al., 1998; Rapaport et al., 1998; Sesaki and Jensen, 2001). To verify the negative interactions, we performed tetrad dissections of the *myo2(LQ)* mutant mated with Δ*fzo1*, Δ*ugo1*, and Δ*mgm1*, which lacks the third core component of the yeast mitochondrial fusion machinery (Wong et al., 2000). No double mutants of the *myo2(LQ)* allele in combination with Δ*fzo1*, Δ*mgm1*, or Δ*ugo1* could be obtained, confirming the synthetic lethality (Fig. 1 H). This ob-

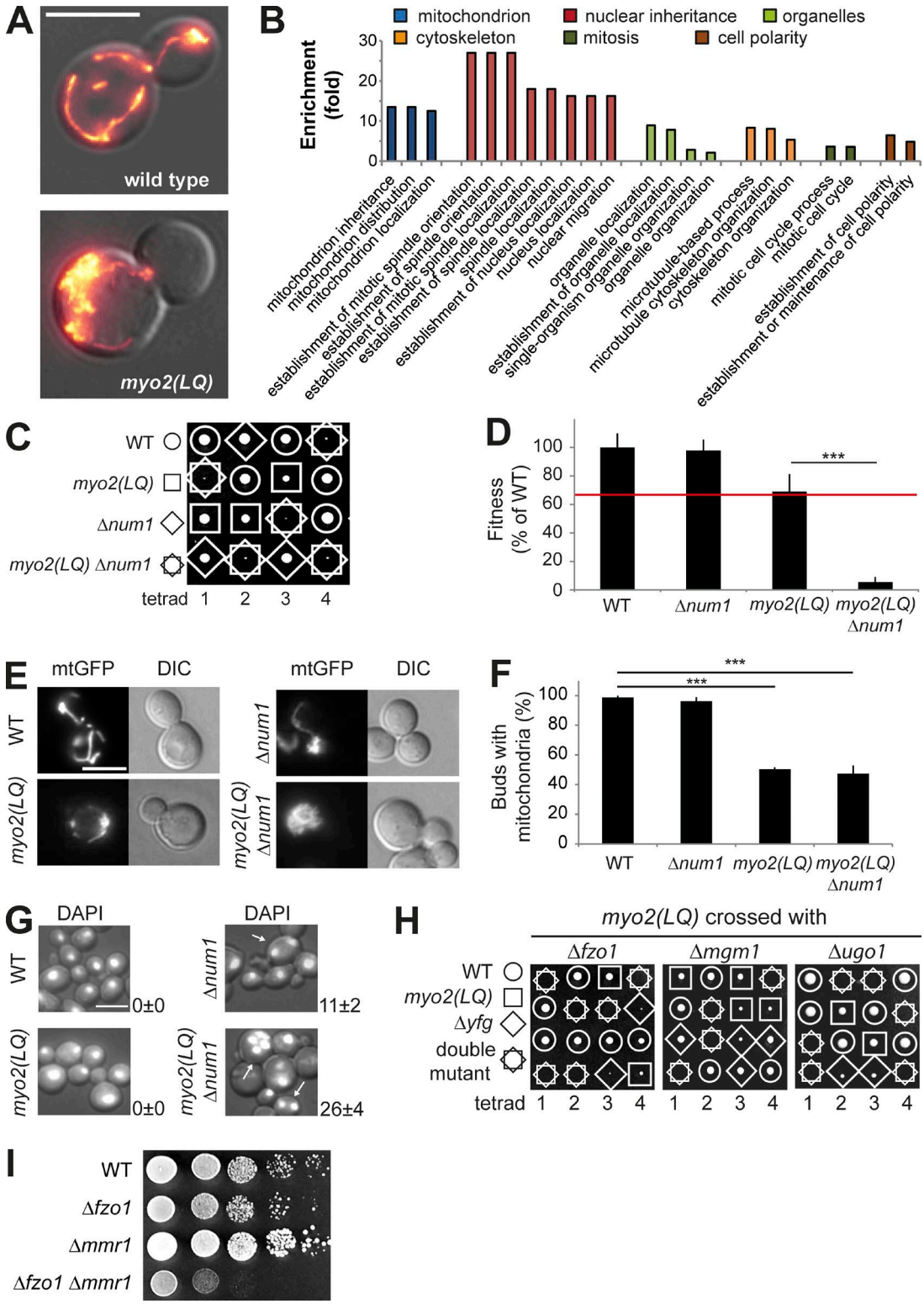

Figure 1. **Genetic interactions of *myo2(LQ)*.** (A) Yeast cells expressing mtGFP were analyzed by fluorescence microscopy. Representative images are DIC merged with maximum intensity projections of z stacks. (B) Negative genetic interactors of *myo2(LQ)* were analyzed for GO term enrichments in the category "process." (C) Tetrads of heterozygous *myo2(LQ)* Δ*num1* cells were dissected on glucose-containing rich medium. (D) The colony size was determined after tetrad dissection and normalized to WT (fitness). The red line marks the expected fitness of the double mutant (i.e., the product of the two single mutants' fitness). (E and F) Cells expressing mtGFP were analyzed by fluorescence microscopy. (G) Cells were fixed, stained with DAPI, and analyzed by fluorescence microscopy. Arrows indicate cells with supernumerary nuclei. The percentage of cells with supernumerary nuclei was scored in at least 100 cells per strain (triplicate experiments ± SD). (H) Strains were crossed as indicated, sporulated, and tetrads were dissected on glucose-containing rich medium. (I) 10-fold serial dilutions of cell suspensions were spotted on glucose-containing rich medium and incubated at 30°C. Bars, 5 µm. Data pooling and statistics are detailed in Table S4.

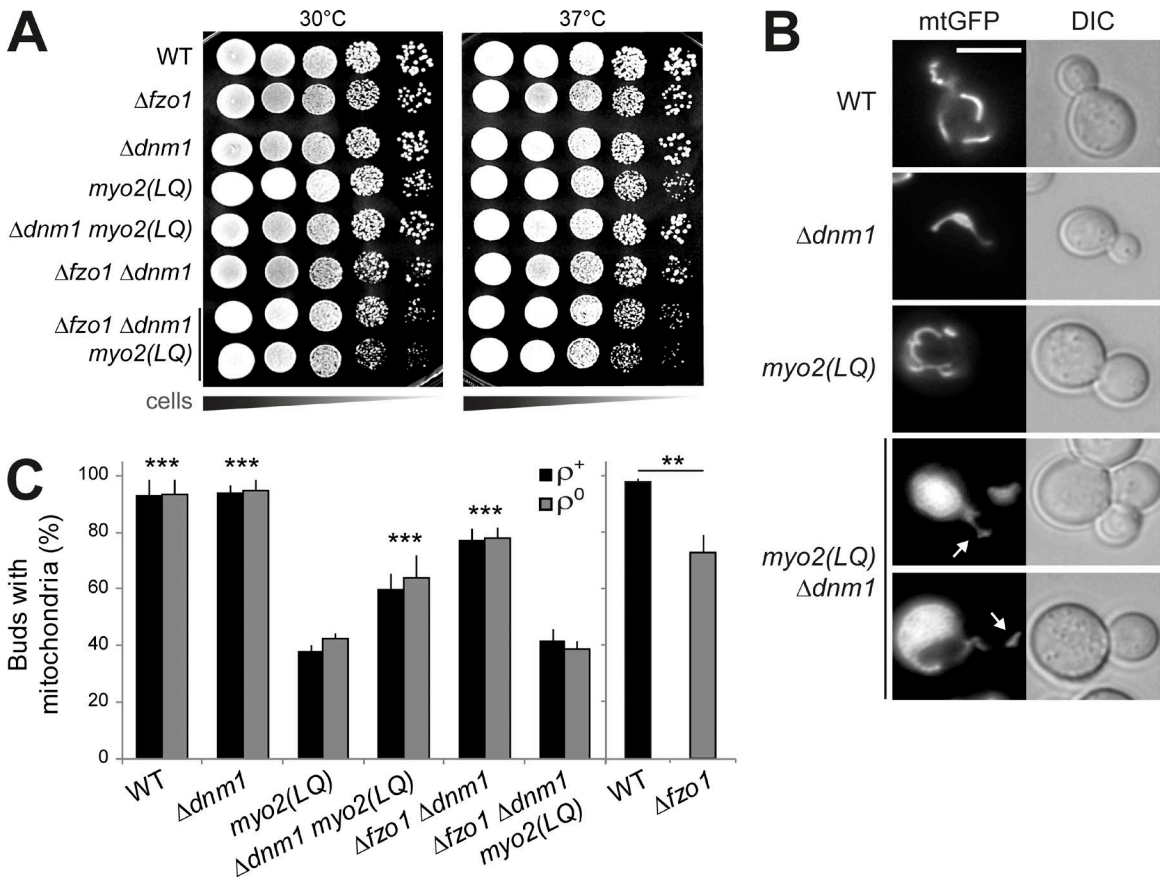

Figure 2. **Rescue of mitochondrial inheritance defects by deletion of the *DNM1* gene.** (A) 10-fold serial dilutions of cell suspensions were spotted on glucose-containing rich medium and incubated at the indicated temperatures. (B) Cells expressing mtGFP were analyzed by fluorescence microscopy. Arrows indicate inherited mitochondria in *myo2(LQ)* Δ*dnm1* cells. Bar, 5 µm. (C) Cells containing (ρ^+, black bars) or lacking mtDNA (ρ^0, gray bars) were analyzed as in B, and buds were scored for the presence of mitochondria. Significance was calculated in comparison to *myo2(LQ)* both for ρ^+ and ρ^0 cells. The Δ*fzo1* mutant is always ρ^0 and was analyzed in a separate experiment and compared with WT. Data pooling and statistics are detailed in Table S4.

servation suggests that fusion becomes a critical factor when bud-directed mitochondrial transport is compromised. As Myo2 has multiple functions in different transport processes, we confirmed this in mutants lacking Mmr1, a factor promoting specifically anterograde transport of mitochondria (Itoh et al., 2004; Swayne et al., 2011; Eves et al., 2012; Chernyakov et al., 2013). Indeed, we found that Δ*mmr1* Δ*fzo1* double mutants have a strong synthetic growth defect (Fig. 1 I). In sum, this shows that a powerful transport machinery is vital for mitochondrial inheritance in fusion mutants.

Mitochondrial inheritance in transport and fusion mutants is improved by fission defects

Dnm1 is the core component of the mitochondrial fission machinery, and mutant cells lacking Dnm1 contain a single, hyperfused mitochondrion (Otsuga et al., 1998). Δ*dnm1* Δ*fzo1* double mutants lack both fusion and fission activity but contain a WT-like tubular mitochondrial network and are able to maintain mtDNA (Bleazard et al., 1999; Sesaki and Jensen, 1999). To test whether the lack of mitochondrial fusion or the presence of small, fragmented mitochondria caused synthetic lethality in the *myo2(LQ)* Δ*fzo1* double mutant, we constructed a *myo2(LQ)* Δ*dnm1* Δ*fzo1* triple mutant and found it viable; i.e., deletion of the *DNM1* gene restores viability of the *myo2(LQ)* Δ*fzo1* mutant. The fact that the triple mutant grows almost like WT (Fig. 2 A) demonstrates that maintenance of tubular mitochondrial morphology, rather than mitochondrial fusion activity, becomes important when Myo2 function is compromised.

Next, we asked whether deletion of the *DNM1* gene is beneficial for mitochondrial inheritance in the *myo2(LQ)* mutant. We found that *myo2(LQ)* Δ*dnm1* cells contained hyperfused mitochondrial networks that frequently carried a tubular extension reaching into the bud (Fig. 2 B). The mitochondrial inheritance defect of *myo2(LQ)* was significantly alleviated by deletion of *DNM1*. The *myo2(LQ)* Δ*dnm1* Δ*fzo1* triple mutant had an inheritance defect similar to *myo2(LQ)*. Interestingly, the Δ*fzo1* mutant also showed a significant mitochondrial inheritance defect. To test the possibility that the presence of the mitochondrial genome plays a role in mitochondrial inheritance, we grew yeast strains on ethidium bromide–containing medium to induce loss of mtDNA (Goldring et al., 1970). All strains grew well on media containing fermentable carbon sources. Quantification of mitochondria in newly formed buds revealed that the absence of mtDNA does not affect mitochondrial inheritance (Fig. 2 C). Our observations suggest that the formation of interconnected mitochondrial networks in fission-defective mutants promotes mitochondrial inheritance when the transport capacity of the Myo2 motor becomes limiting.

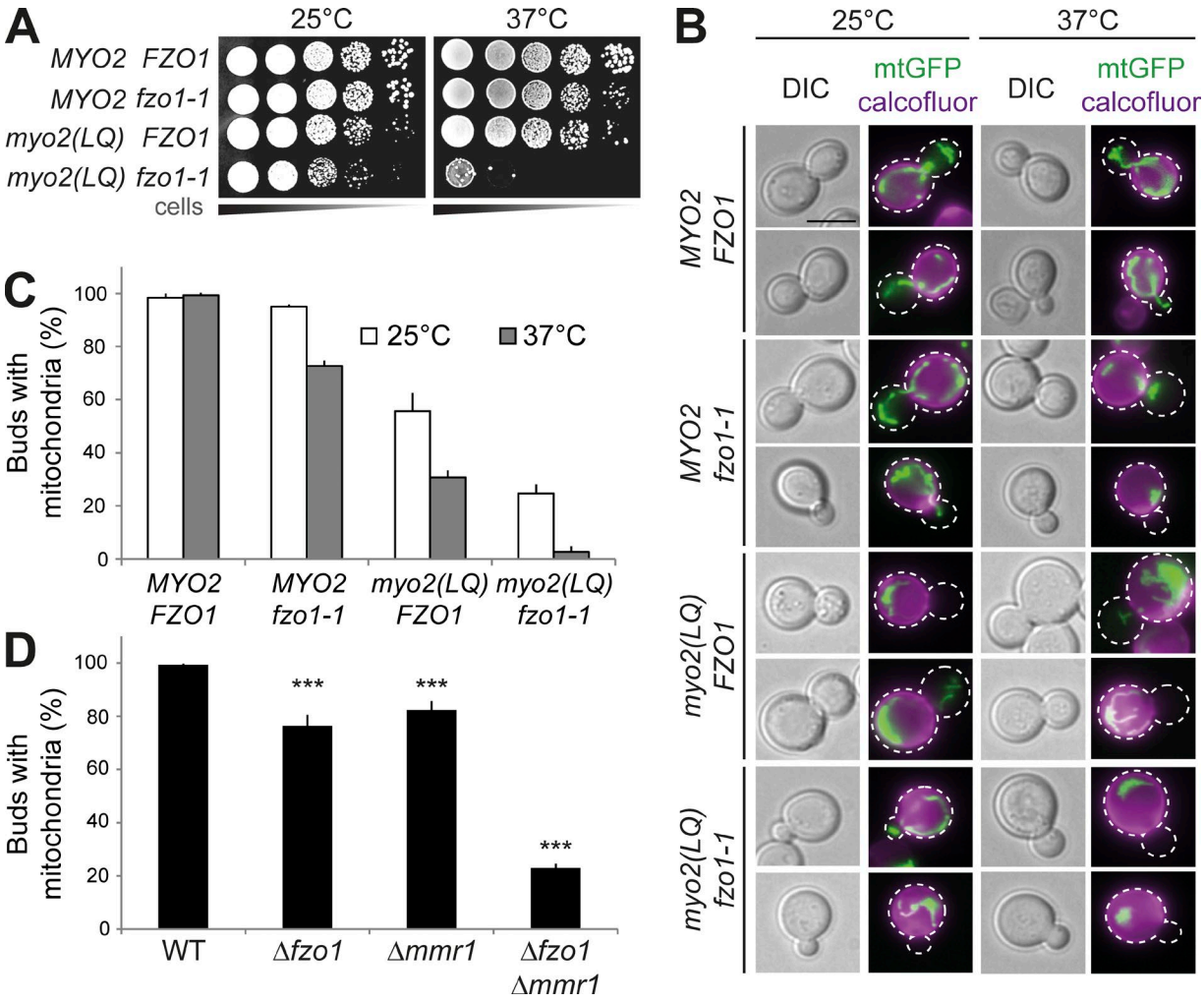

Figure 3. **Defective mitochondrial inheritance in transport and fusion mutants.** (A) 10-fold serial dilutions of cell suspensions were spotted on glucose-containing rich medium and incubated at the indicated temperatures. (B–D) Cells expressing mtGFP were grown at 25°C, cell walls were stained with calcofluor, cultures were split and incubated at the indicated temperatures for 1.5 h, and mitochondrial inheritance was scored. Bar, 5 µm. Data pooling and statistics are detailed in Table S4.

Mitochondrial fusion becomes essential when bud-directed transport is compromised

To observe the behavior of fusion-defective mitochondria in the *myo2(LQ)* background, we made use of the temperature-sensitive *fzo1-1* allele, which leads to rapid fragmentation of the mitochondrial network and inability to grow on nonfermentable carbon sources at 37°C (Hermann et al., 1998). As expected, the *myo2(LQ) fzo1-1* double mutant grows well at 25°C but is almost inviable at 37°C (Fig. 3 A). To analyze mitochondrial inheritance, we incubated cells expressing mitochondria-targeted GFP (mtGFP) at permissive temperature (25°C) and stained the cell wall with calcofluor to allow the identification of mother cells. Then, cultures were split and incubated for 1.5 h at permissive and nonpermissive (37°C) temperature, and mitochondrial inheritance was quantified in newly formed buds lacking calcofluor staining. Consistent with previously published observations (Förtsch et al., 2011), the *myo2(LQ)* mutant was observed to have a pronounced mitochondrial inheritance defect at 25°C, which was even more severe at 37°C. The *fzo1-1* mutant has a moderate inheritance defect at the nonpermissive temperature. Strikingly, only ∼20% of *myo2(LQ) fzo1-1* double mutant buds contained mitochondria at 25°C, and mitochondrial inheritance was almost completely blocked at 37°C (Fig. 3, B and C). As mitochondrial inheritance is essential for viability, this defect explains the observed synthetic lethality of *myo2(LQ)* Δ*fzo1* cells.

To obtain independent evidence for a link of mitochondrial fusion and transport, we quantified mitochondrial inheritance in buds of Δ*fzo1*, Δ*mmr1*, and Δ*fzo1* Δ*mmr1* cells. Although each single mutant showed only a moderate inheritance defect, mitochondria could be detected in only ∼20% of Δ*fzo1* Δ*mmr1* buds (Fig. 3 D). We conclude that mitochondrial inheritance is severely disturbed when mitochondrial fusion and anterograde transport are simultaneously compromised.

Fragmented mitochondria have an inheritance defect at the step of transfer from the mother to the daughter cell

Recently, it was proposed that Fzo1 contributes to mitochondrial inheritance by fusion of newly inherited mitochondria to a continuous mitochondrial reticulum that remains anchored at the bud tip. This activity was suggested to increase the mitochondrial quantity in the bud by preventing retrograde move-

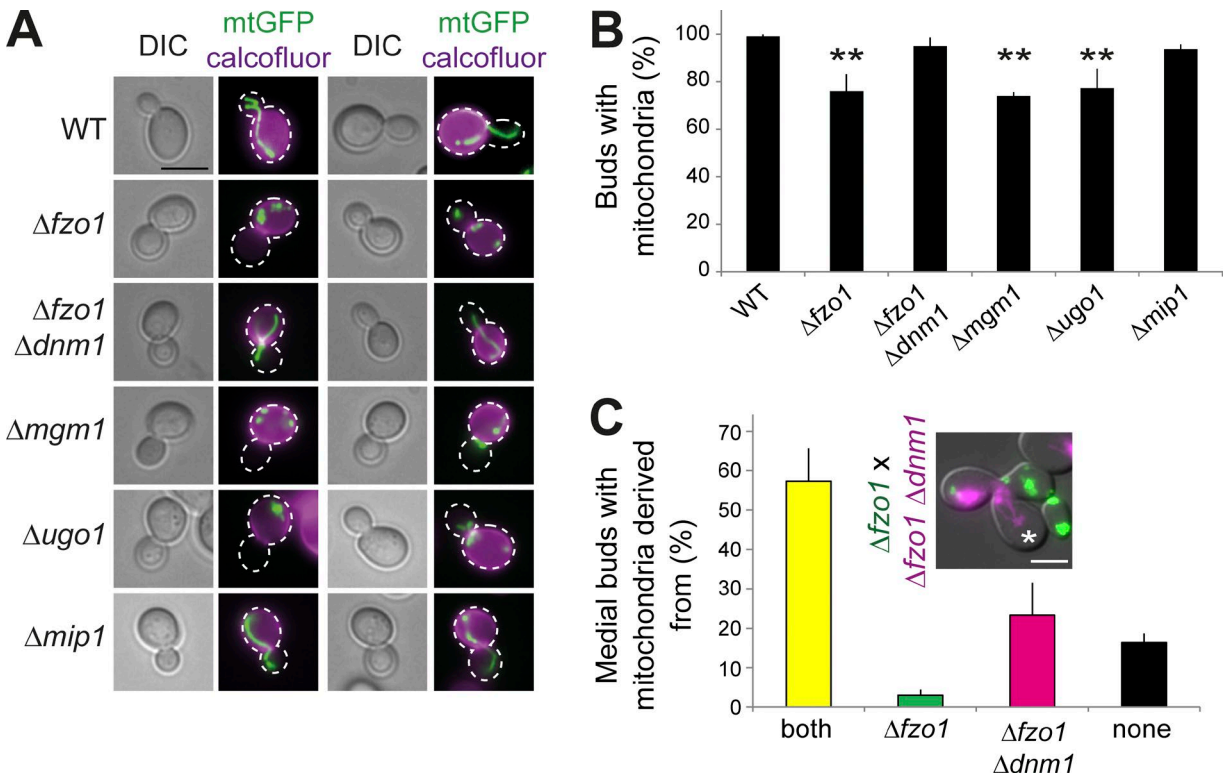

Figure 4. **Mitochondrial inheritance defects of fragmented mitochondria.** (A and B) Cells were analyzed as in Fig. 3 (B–D) at 30°C. Bar, 5 µm. (C) Δ*fzo1* cells expressing mtGFP and Δ*fzo1* Δ*dnm1* cells expressing mtERFP from galactose-inducible promoters were grown overnight in galactose-containing selective complete medium supplemented with 1% raffinose, washed in glucose-containing rich medium, and equal amounts of cells mixed. Cells were allowed to mate for 5 h in glucose-containing rich medium, fixed with formaldehyde, and mitochondrial inheritance to medial buds analyzed. A representative image shows a zygote inheriting mitochondria only from the Δ*fzo1* Δ*dnm1* parent. The asterisk indicates the bud. Bar, 5 µm. Data pooling and statistics are detailed in Table S4.

ments back into the mother cell (Higuchi-Sanabria et al., 2016). A possible reduction of the rate of fusion-deficient mitochondria entering the bud was not reported. We considered the possibility that the presence of fused mitochondria is important already at the step of transport across the bud neck before mitochondria reach the bud tip. To test this idea, we examined mitochondrial behavior in transport- and fusion-defective mutants by live-cell microscopy. Cells expressing mtGFP were continuously supplied with fresh medium and observed for 1 h. In WT cells, mitochondria were observed to frequently move in the anterograde direction and cross the bud neck early after bud emergence (Video 1). In contrast, mitochondria of *fzo1-1* cells incubated at nonpermissive temperature first accumulate at the bud neck before they enter the bud relatively late in the cell cycle (Video 2). Consistent with previous observations (Förtsch et al., 2011), mitochondrial movement is largely restricted to the mother cell in *myo2(LQ)* mutants where only few mitochondria reach the bud (Video 3). Strikingly, we could not detect any mitochondria in buds of *myo2(LQ) fzo1-1* cells under nonpermissive conditions. Instead, mitochondria accumulate at the mother cell pole opposite the bud and show only little movement (Video 4), indicating a complete block of inheritance.

Again, we confirmed this synthetic defect using Δ*fzo1* and Δ*mmr1* deletion alleles. Mitochondrial behavior was normal in WT cells (Video 5), and mitochondria readily crossed the bud neck in Δ*mmr1* (Video 6) and eventually also in Δ*fzo1* (Video 7). In contrast, there was hardly any bud-directed mitochondrial movement in the Δ*fzo1* Δ*mmr1* double mutant (Video 8). These results are consistent with the quantifications of mitochondrial inheritance shown above (Fig. 3) and suggest that fused mitochondria are important for their transfer across the bud neck, rather than accumulation at the bud tip.

To test whether there is a general mitochondrial inheritance defect in mitochondrial fusion-deficient strains even in the presence of WT *MYO2*, we quantified mitochondrial inheritance to newly formed buds. We observed a mitochondrial inheritance defect in all fusion-deficient mutants tested (Δ*fzo1*, Δ*mgm1*, and Δ*ugo1*). This defect was rather mild (i.e., 70% to 80% of buds received mitochondria) but significant (Fig. 4, A and B). It was not caused by the loss of mtDNA, because mitochondrial inheritance was not affected in the Δ*mip1* mutant lacking the mtDNA polymerase (Fig. 4, A and B). The inheritance defect could be relieved by simultaneous block of fusion and fission in Δ*fzo1* Δ*dnm1* (Fig. 4, A and B), suggesting that the fragmented state of mitochondria is the main reason for less efficient inheritance in mitochondrial fusion mutants.

Next, we tested mitochondrial inheritance in a competition experiment in zygotes. Δ*fzo1* cells stained with mtGFP were mated with Δ*fzo1* Δ*dnm1* cells stained with mitochondria-targeted enhanced RFP (mtERFP), and inheritance of mitochondria from parental cells to the bud was quantified in zygotes. Approximately 55% of the buds received mitochondria from both parental cells, and ∼17% of the buds were devoid of mitochondria. A comparison of the buds that had received mitochondria from only one parent revealed a striking difference: ∼25% of the buds contained tubular mitochondria inherited only from the Δ*fzo1* Δ*dnm1* parent, whereas only 3% of the buds contained fragmented mitochondria inherited only from the Δ*fzo1*

parent (Fig. 4 C). In sum, we conclude that fragmented mitochondria are less likely to be inherited to the daughter cell.

A model simulating the inheritance of tubular versus fragmented mitochondria

We developed a simplified model to simulate bud-directed transport of mitochondrial particles with varying affinity to the motor protein. In brief, our model considers a mother yeast cell and a daughter cell (both having fixed diameters of 5 µm) with transport of mitochondria being restricted to the one-dimensional axis from the mother to the daughter cell pole. Two mitochondrial particles were assumed to be anchored at the mother cell pole by the Num1 plasma membrane anchor. This situation corresponds to the number of attachment sites that can be observed in vivo when bud-directed mitochondrial movement is enforced (Klecker et al., 2013). All other particles were allowed to diffuse and be picked up by anterograde and retrograde transport systems along the axis with rate k_{on}, whereas dissociation from the transport machinery was considered via rate k_{off}. Mitochondrial movement along actin filaments was modeled at a constant velocity of 0.4 µm/s, which is compatible with the speed of mitochondrial movements observed in vivo (Fehrenbacher et al., 2004). Mitochondrial partitioning was allowed for a simulated time of 120 min, corresponding to the generation time of yeast.

To mimic mitochondrial networks in the WT, we assumed the presence of two flexible mitochondrial tubules, each being represented by a flexible linear chain of 19 particles, with the first particle being anchored to the mother cell pole by Num1. For Δ*fzo1* mutants, we assumed instead a total number of 38 isolated particles, again with two particles being anchored to the mother cell pole. Individual particles were assumed to be 550 nm long with a mutual excluded-volume interaction while being subject to anterograde and retrograde transport. The *myo2(LQ)* mutation was mimicked by an increased dissociation rate, k_{off}. We arbitrarily assumed that daughter cells have to receive at least 15% of the available mitochondrial mass for survival. We performed 200 simulations for each parameter condition and used these data to obtain the mean number of mitochondrial particles at each lattice site along the mother–bud axis over time.

The simulation suggests that inheritance of both tubular and fragmented mitochondria is supported when the k_{off} rate of the anterograde motor is reasonably low, corresponding to the presence of a WT *MYO2* allele. Inheritance of a critical mass of mitochondria to the bud is much more resistant against perturbations of motor binding when tubular mitochondria are present. In other words, a relatively high affinity of the motor to its cargo is required when mitochondria are fragmented, and a combination of fragmented mitochondria with a weakly binding motor protein causes a drop of the mitochondrial quantity transferred to the bud below a critical threshold (Fig. 5 A). These predictions fit very well to the experimental results described above (Fig. 3). During the simulation of bud-directed transport of fragmented mitochondria, we noticed that mitochondria initially pile up at the bud neck before they enter the bud (Fig. 5 B). Also, this observation fits to our experimental data (Video 2).

The model predicts that viability of fusion-deficient mutants can be restored by an increased affinity of the motor to mitochondria. To test this idea, we overexpressed the *YPT11* gene in *myo2(LQ) fzo1-1* cells. Ypt11 is a small Rab GTPase that is thought to promote mitochondrial transport by supporting Myo2 binding to mitochondria (Itoh et al., 2002; Chernyakov et al., 2013; Lewandowska et al., 2013). As a control, we also tested the *ypt11(G40D)* allele, which encodes an inactive Ypt11 variant with a mutation in its GTPase domain (Itoh et al., 2002). Indeed, growth of *myo2(LQ) fzo1-1* was markedly improved by overexpression of Ypt11, but not Ypt11(G40D) (Fig. 5 C). Microscopy confirmed that overexpression of Ypt11 improved mitochondrial inheritance in *myo2(LQ)* (Fig. 5, D and E). In an alternative approach, we expressed Myo2-Fis1 in a Δ*fzo1* Δ*mmr1* double mutant strain. Myo2-Fis1 is mitochondria-specific motor protein carrying a Fis1 mitochondrial outer membrane anchor replacing the C-terminal cargo-binding domain. Expression of this chimeric protein does not affect the distribution of vacuoles, secretory vesicles, Golgi, and ER (Förtsch et al., 2011). Growth of the double mutant was significantly improved by the presence of this motor, which is permanently bound to mitochondria (i.e., $k_{off} = 0$) and promotes accumulation of mitochondria in the bud (Fig. 5 F). It should be noted that Myo2-Fis1 was not overexpressed in this experiment which would be predicted to deplete mother cells from mitochondria (see also Fig. 6). We conclude that the model reliably predicts the behavior of mitochondria when the fused state or the affinity to the motor is altered. In sum, our observations suggest that faithful mitochondrial inheritance depends on the coordinated action of the mitochondrial fusion, fission, and transport machineries.

Fusion enables retention of mitochondria in the mother cell when anterograde transport is enforced

The simulation also suggested that fusion-deficient mother cells are depleted from mitochondria when the affinity of the motor to mitochondria is increased (Fig. 5 A). To test this, we expressed Myo2-Fis1, which is permanently bound to mitochondria, from an inducible promoter in fusion mutants. Δ*fzo1* cells were viable when the promoter was shut off, but inviable when Myo2-Fis1 was expressed (Fig. 6 A). Only a minor growth defect was observed when Myo2-Fis1 was expressed in Δ*mip1* cells lacking mtDNA (Fig. 6 A). Consistent with earlier observations (Förtsch et al., 2011; Klecker et al., 2013), overexpression of Myo2-Fis1 in WT or Δ*mip1* cells led to the accumulation of mitochondria in the bud, whereas one or two long mitochondrial tubules remained in the mother cell (Fig. 6, B and C). In contrast, induction of Myo2-Fis1 expression led to depletion of 20% of the Δ*fzo1* mother cells from mitochondria (Fig. 6, B and C). This is in very good agreement with the model (Fig. 5 A). We conclude that enforced bud-directed mitochondrial transport kills fusion-deficient mother cells because they cannot retain a critical mitochondrial quantity.

To further confirm this conclusion, we asked whether fusion-deficient cells tolerate enforcement of bud-directed mitochondrial transport by overexpression of Ypt11. WT, Δ*fzo1*, and Δ*fzo1* Δ*dnm1* cells were transformed with plasmids overexpressing the *YPT11* gene or the inactive *ypt11(G40D)* variant from the constitutive *GPD* promoter or an empty vector control. In addition, they contained the WT *FZO1* gene on a plasmid with an *URA3* marker to allow counterselection against the plasmid on medium with 5-fluoroorotic acid (5-FOA). We observed that Δ*fzo1* cells overexpressing Ypt11, but not Ypt11(G40D), were unable to grow on 5-FOA–containing medium (Fig. 6 D). This means that the *FZO1* gene becomes essential when the *YPT11* gene is overexpressed. The fact that Δ*fzo1* Δ*dnm1* cells are insensitive to Ypt11 overexpression suggests that the shape

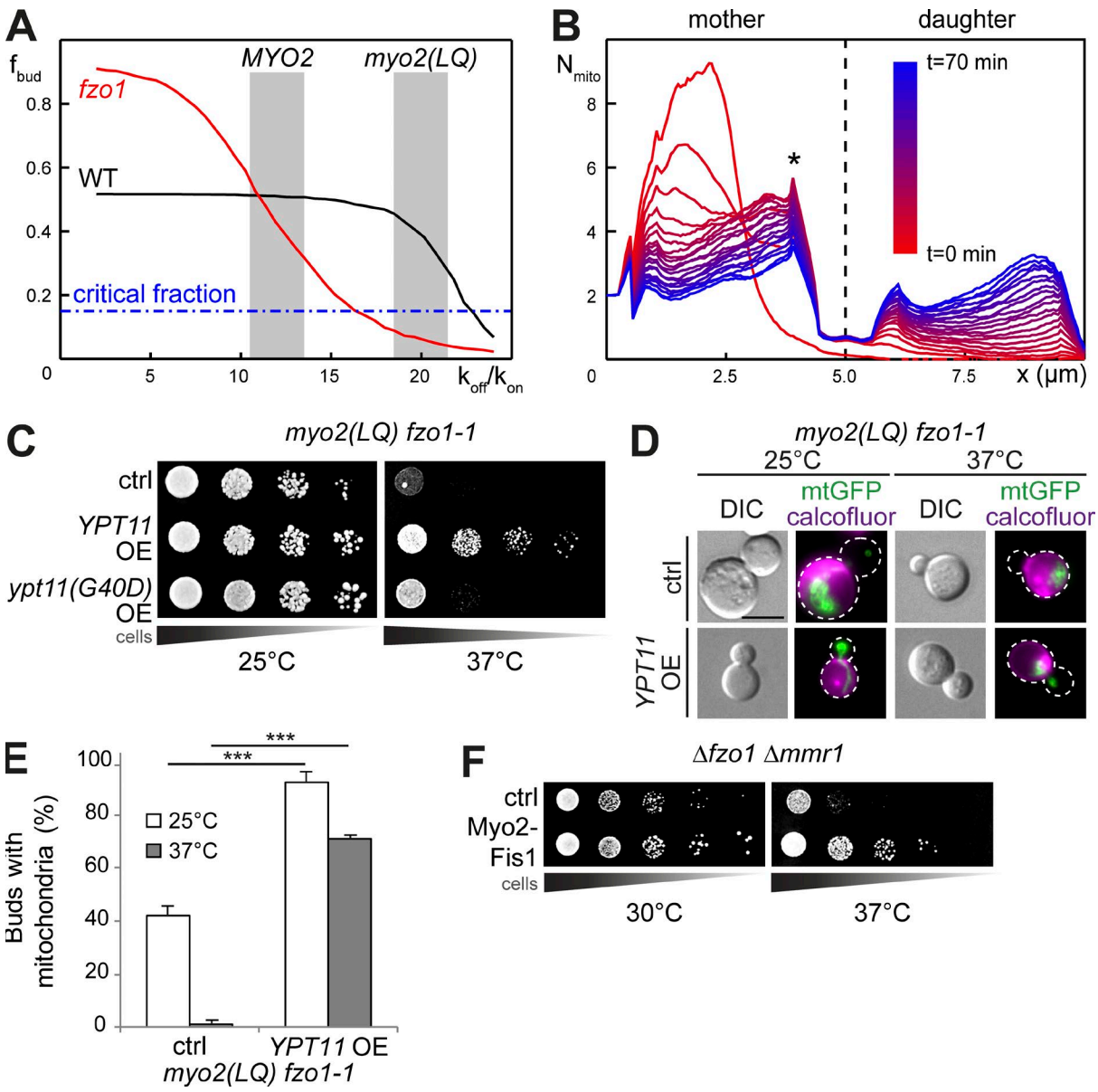

Figure 5. **Modeling mitochondrial transport.** (A) Simulation of the decline of mitochondrial quantity that reaches the bud (f_{bud}) when the dissociation rate from the actin track (k_{off}) is enhanced. Gray shaded regions indicate normal (*MYO2*) or increased (*myo2(LQ)*) k_{off} rates. For simplicity, we have assumed that daughter cells require at least 15% of the initial mitochondrial mass (blue dashed–dotted line). The dissociation rate k_{off} is depicted relative to the corresponding association rate, k_{on}. (B) The distribution of fragmented mitochondria (N_{mito}) along the mother–bud axis (x) in Δ*fzo1* cells was simulated as in A and depicted in a time-resolved presentation. The asterisk marks a transient accumulation of mitochondria at the bud neck. (C) 10-fold serial dilutions of *myo2(LQ) fzo1-1* cells carrying a vector control (ctrl) or overexpressing *YPT11* or *ypt11(G40D)* from a *GPD* promoter (OE) were spotted on glucose-containing selective medium and incubated at the indicated temperatures. (D and E) Cells were analyzed as in Fig. 3 (B and C). Bar, 5 µm. (F) Δ*fzo1* Δ*mmr1* cells expressing Myo2-Fis1 from the *MYO2* promoter on a single-copy plasmid or carrying a vector control (ctrl) were analyzed as in C. Data pooling and statistics are detailed in Table S4.

and size of mitochondria, rather than their fusion activity, is important. In sum, our observations indicate that mother cells containing tubular mitochondria are more resistant against depletion from mitochondria than mutants containing fragmented mitochondria. Thus, fusion plays an important role not only in mitochondrial inheritance to the bud but also in retention in the mother cell.

Compromised mitochondrial transport affects replicative lifespan

Inhibition of mitochondrial transport in *myo2(LQ)* cells leads to highly asymmetric mitochondrial distribution in mother and daughter cells (Förtsch et al., 2011; see also Figs. 1, 2, and 3). To test whether this affects replicative lifespan, we isolated virgin cells using a micromanipulator and determined the number of daughters these cells produced before they died (Park et al., 2002). A Δ*sir2* mutant, lacking a NAD^+-dependent histone deacetylase of the sirtuin family, was included in this analysis as a control, because this strain is known to have a shortened replicative lifespan (Kaeberlein et al., 1999). We found that the mean lifespan of Δ*sir2* and *myo2(LQ)* cells was strongly reduced in comparison to the WT (Fig. 7 A). Strikingly, ∼70% of the *myo2(LQ)* cells were very short-lived and ceased to produce new buds after less than five divisions, whereas a few cells were very long-lived (Fig. 7,

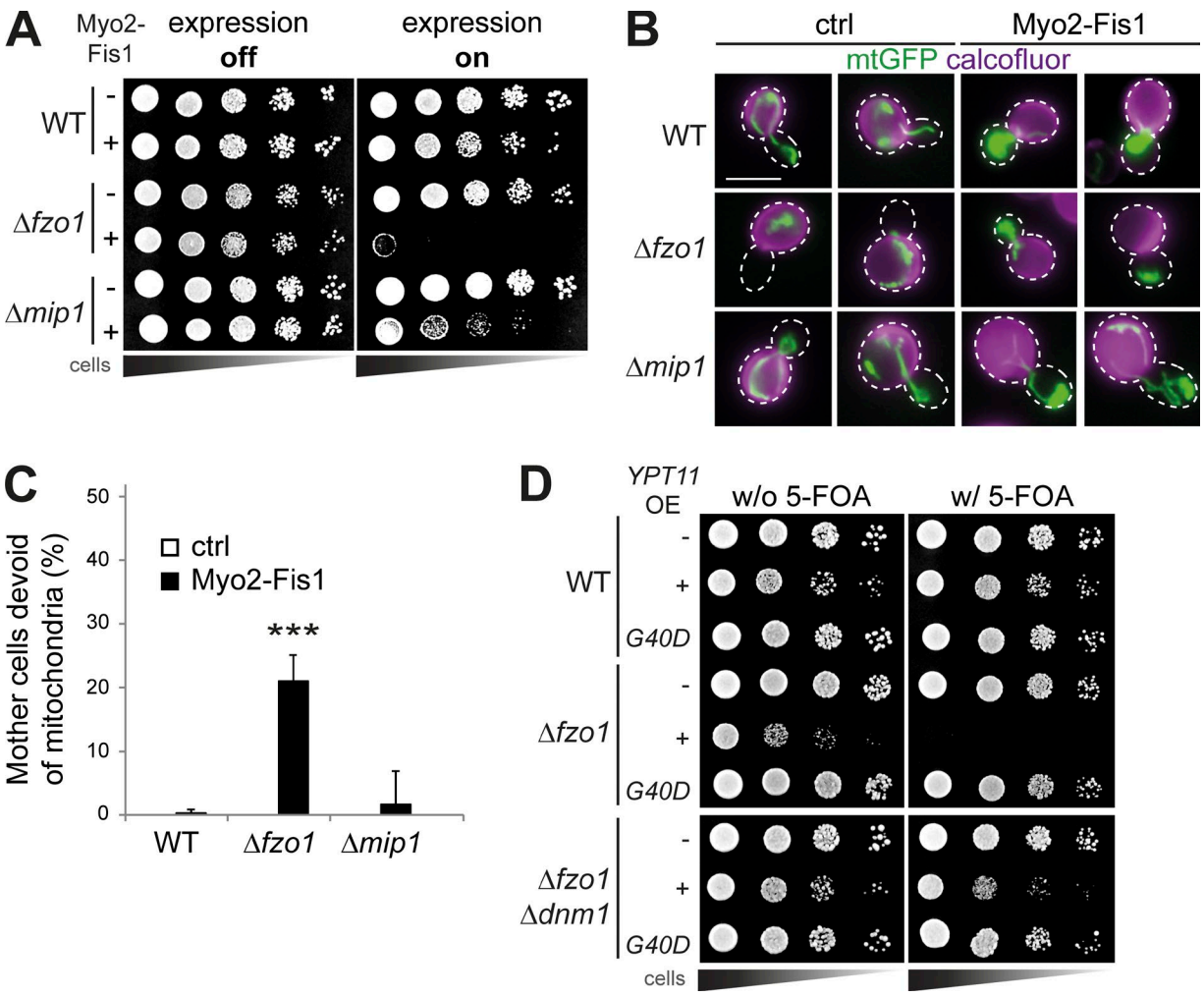

Figure 6. **Mitochondrial retention defects of fragmented mitochondria.** (A) 10-fold serial dilutions of cells carrying a plasmid expressing Myo2-Fis1 from a *tetO* promoter (+) or a vector control (–) were spotted on glucose-containing selective medium with (off) or without (on) doxycycline and incubated at 30°C. (B) Cells carrying a vector control (ctrl) or a plasmid expressing Myo2-Fis1 from a *GAL* promoter were grown in galactose-containing synthetic complete medium supplemented with 0.5% glucose and analyzed as in Fig. 4 A. Bar, 5 µm. (C) Cells prepared as in B were scored for mother cells completely lacking mitochondria. (D) *FZO1* WT cells, Δ*fzo1*, and Δ*fzo1* Δ*dnm1* cells containing a plasmid carrying WT *FZO1* and a *URA3* marker received as a second plasmid either an empty vector (–) or plasmids overexpressing *YPT11* (+) or *ypt11(G40D)* from a *GPD* promoter. Strains were first allowed to lose the *FZO1* plasmid in selective medium containing uracil. Then, 10-fold serial dilutions were spotted on glucose-containing selective medium with or without 5′-FOA, which counterselects against cells that have maintained the *FZO1* plasmid. Data pooling and statistics are detailed in Table S4.

B and C). Although we cannot exclude the possibility that noninherited mitochondria accumulating in mother cells cause lifespan problems, we consider it more likely that buds that fail to inherit a critical mitochondrial quantity are destined to die.

The *myo2(LQ)* mutation also compromises the inheritance of vacuoles (Förtsch et al., 2011), and declining vacuolar acidity in aged cells was shown to negatively affect lifespan and mitochondrial function (Hughes and Gottschling, 2012). To test whether Myo2-dependent vacuolar inheritance defects reduce replicative lifespan, we examined the vacuole-specific *myo2(D1297N)* mutant (Catlett et al., 2000). Consistent with previous observations (Altmann et al., 2008; Eves et al., 2012), we confirmed that *myo2(D1297N)* cells have a severe vacuolar inheritance defect but WT-like mitochondrial inheritance (Fig. 7, D–F). The lifespan of *myo2(D1297N)* cells was indiscernible from that of the WT, suggesting that Myo2-dependent transport of vacuoles plays only a minor role (Fig. 7 G).

Our results suggest that each generation of *myo2(LQ)* mother cells produces a fraction of buds that receive a less than critical mitochondrial quantity and therefore cannot sustain growth of more than very few buds. To confirm this, we tested whether the inviability of daughter cells can be rescued by restoration of mitochondrial inheritance. We observed that overexpression of *YPT11* restored both mitochondrial inheritance and viability of newly born daughter cells in *myo2(LQ)* (Fig. 7, H–J). In sum, we propose that the inheritance of a critical mitochondrial quantity is a crucial factor determining the replicative lifespan of yeast.

Myo2-dependent transport of mitochondria is important for retention of cytosolic protein aggregates

Heat stress–induced cytosolic protein aggregates were shown to be associated with mitochondria and retained in the mother cell (Zhou et al., 2014). We asked whether this process is dependent on mitochondrial dynamics and Myo2. To test this, we stained the yeast mother cell wall with calcofluor, subjected the cells to a heat shock for 5 min at 42°C, and allowed the formation

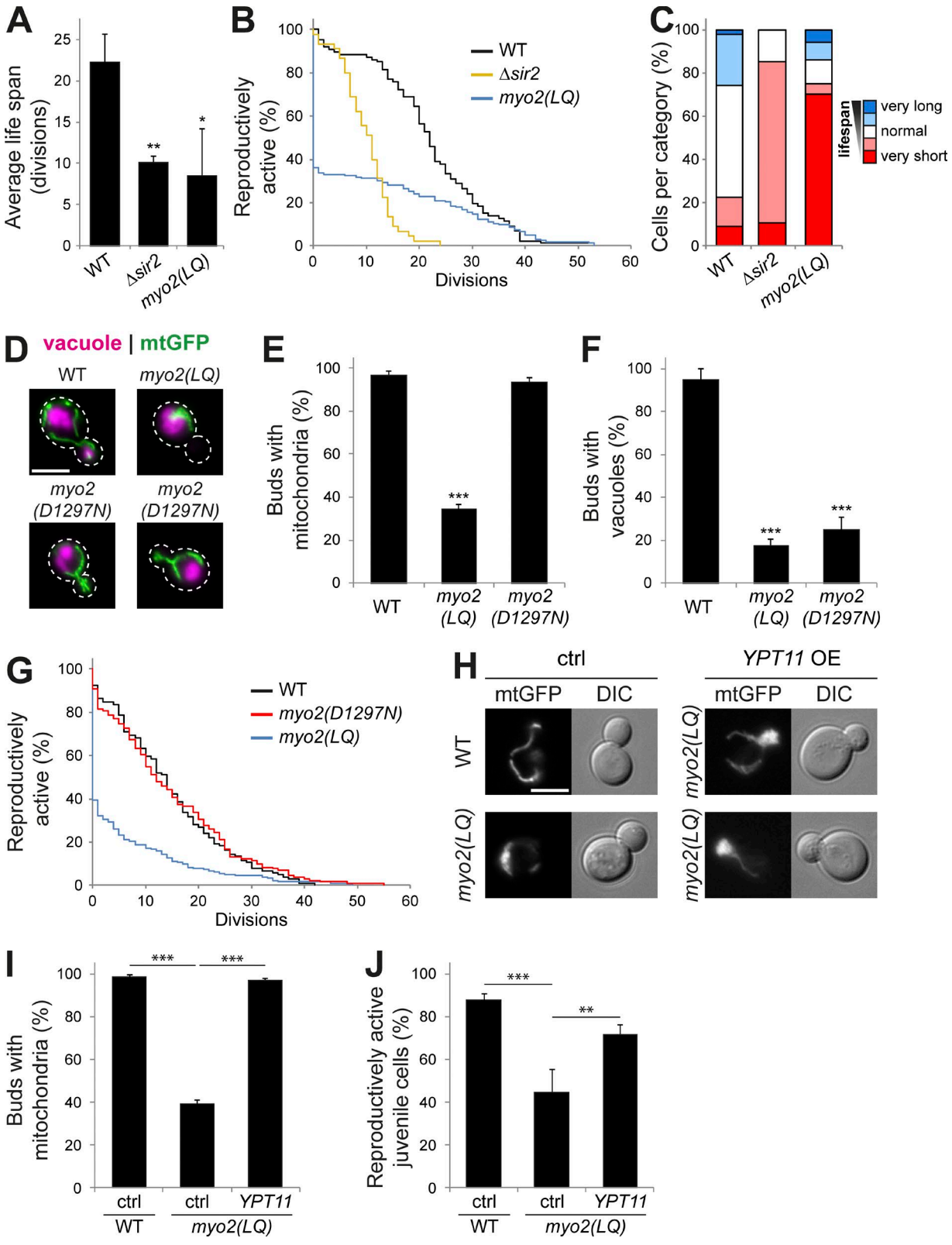

Figure 7. **Replicative lifespan of *myo2* mutants.** (A–C) Replicative lifespan (RLS) of WT (n = 87), Δ*sir2* (n = 45), and *myo2(LQ)* (n = 163) was analyzed in three independent experiments with at least 12 cells per strain in each experiment. Mean values are shown in A. A RLS analysis representing the pooled values of the same experiments is shown in B. In C, cells were grouped into the following categories: very short lived (0–4 divisions), short-lived (5–14 divisions), normal (15–29 divisions), long-lived (30–39 divisions), and very long-lived (40–70 divisions). (D–F) Inheritance of vacuoles and mitochondria was analyzed in Δ*myo2* cells containing plasmids expressing *MYO2*, *myo2(LQ)*, or *myo2(D1297N)* from the *MYO2* promoter. (G) RLS analysis was performed as in B; *MYO2* (n = 104), *myo2(LQ)* (n = 180), *myo2(D1297N)* (n = 131). (H and I) Inheritance of mitochondria was analyzed in cells containing either an empty vector (ctrl) or overexpressing *YPT11* from the *GPD* promoter. Bar, 5 µm. (J) Strains were grown on selective media plates, individual cells were arrayed on a grid, mother cells were removed after the first division, and juvenile cells were scored for their ability to produce colonies. Bars, 5 µm. Data pooling and statistics are detailed in Table S4.

of new buds at 30°C for 2–3 h. Heat-induced cytosolic protein aggregates were labeled with a GFP fusion of $Hsp104^{Y662A}$, an enzymatically inactive chaperone that stably binds to protein aggregates but fails to resolve them (Lum et al., 2004; Zhou et al., 2011). Consistent with the observations of Zhou et al. (2014), we observed in WT cells that protein aggregates colocalized with mitochondria and that 80% of the cells retained all aggregates in the mother (Fig. 8, A and B). Intriguingly, enforcement of bud-directed mitochondrial transport by expression of Myo2-Fis1 reduced the aggregate retention efficiency to 50% (Fig. 8, A and B). Strikingly, almost all cells that showed a massive accumulation of mitochondria in the bud also contained aggregates in the bud (Fig. 8 A), and in more of 90% of these buds, aggregates were associated with mitochondria (Fig. 8 C). This is strong evidence for an active role of mitochondria in partitioning of cytosolic protein aggregates.

Next, we tested whether the machineries of mitochondrial transport and dynamics are required for aggregate retention. Aggregate retention efficiency was reduced to ∼30% in *myo2(LQ)* but was not significantly affected in Δ*dnm1*, Δ*fzo1*, and Δ*dnm1* Δ*fzo1* (Fig. 8 D). Apparently, mitochondrial fusion and fission activities are not required for aggregate retention, whereas a loss of bud-directed mitochondrial transport allows cytosolic aggregates to enter the bud.

We were puzzled by the observation that both enforcement and restriction of bud-directed mitochondrial transport reduce the aggregate retention efficiency. We considered the possibility that the *myo2(LQ)* mutant fails to retain aggregates because its mitochondria accumulate in the mother away from the bud neck. This could allow the aggregates to enter the bud without being captured by mitochondria. To test this idea, we quantified the buds that contained heat-induced aggregates not associated with mitochondria. Indeed, *myo2(LQ)* cells contained a strongly increased number of buds with aggregates that were not associated with mitochondria (Fig. 8, E and F).

As previous studies suggested that the vacuole might be involved in retention of aggregated proteins (Spokoini et al., 2012; Hill et al., 2016), we again made use of the *myo2(D1297N)* mutant, which has a specific vacuolar inheritance defect. We found that aggregate retention efficiency was not compromised in this strain (Fig. 8, G and H). Also, very few buds contained protein aggregates that were not associated with mitochondria (Fig. 8 I). These observations suggest that vacuolar inheritance defects are not responsible for Myo2-dependent protein aggregate retention phenotypes.

In sum, we propose that on the one hand, a minimal activity of Myo2 is required to distribute mitochondria in the mother cell and allow capture of the aggregates, which is a prerequisite for aggregate retention. On the other hand, an increased activity of Myo2 shifts mitochondria-associated aggregates into the bud and thereby perturbs aggregate retention. Thus, fine-tuned Myo2-dependent mitochondrial transport is critical for retention of cytosolic protein aggregates in the mother cell.

Discussion

Our observations in vivo and simulations in silico revealed a novel role of mitochondrial fusion in inheritance. The transport capacity of WT Myo2 obviously is sufficient for the inheritance of a critical quantity of fragmented mitochondria in Δ*fzo1* cells to sustain viability of most progeny. However, when the transport capacity in *myo2(LQ)* Δ*fzo1* cells is compromised, both the number of successful transport events and the mitochondrial mass transported with each event are reduced, leading to a lethal inheritance defect. This can be partially rescued by deletion of the *DNM1* gene, which increases the size of individual mitochondria that are transported to the bud with each successful transport event. When bud-directed transport is enforced by expression of Myo2-Fis1 or overexpression of Ypt11, maintenance of a critical mitochondrial size becomes important for retention of mitochondria in the mother. Thus, mitochondria must be in a fused state to ensure partitioning of a critical quantity of mitochondria to the bud when the transport capacity of Myo2 becomes limiting. Similarly, fused mitochondria ensure retention of a critical mitochondrial quantity in the mother cell when bud-directed transport is enforced. We conclude that the concerted action of mitochondrial fusion, fission, and Myo2-dependent transport determines mitochondrial partitioning and inheritance in asymmetrically dividing yeast cells.

It was previously suggested that mitochondrial fusion plays a role in mitochondrial quantity control at the bud tip by generating a continuous reticulum of mitochondria that remain anchored in the bud tip (Higuchi-Sanabria et al., 2016). However, this model is inconsistent with several of our observations. We propose here that the shape and size of mitochondria, rather than their fusion activity, is important for mitochondrial inheritance for the following reasons. First, Δ*dnm1* Δ*fzo1* double-mutant cells efficiently inherit mitochondria, even though they completely lack fusion activity. Second, lethality of the *myo2(LQ)* Δ*fzo1* mutant is rescued by deletion of the *DNM1* gene without restoration of mitochondrial fusion activity. Third, time-resolved microscopy and simulations revealed that fusion-defective mutants show mitochondrial transport and inheritance defects already in the mother cell. Fourth, fused mitochondria are important not only for partitioning to the bud but also for retention in the mother. Overall, our data support a model in which mitochondrial fusion and fission dynamics determines the size of mitochondrial units that are transported to the bud or retained in the mother, respectively.

Impaired mitochondrial transport dramatically shortens the mean replicative lifespan of yeast cells. It was previously observed that Δ*mmr1* and Δ*ypt11* mutants produce an increased number of short-lived cells (McFaline-Figueroa et al., 2011; Rafelski et al., 2012). This phenotype was explained by a possible accumulation of lower-functioning mitochondria in some mother cells and taken as evidence for a role of the machinery of mitochondrial inheritance in mitochondrial quality control (McFaline-Figueroa et al., 2011). However, we consider it unlikely that rather subtle differences of redox potential in individual mitochondria can be responsible for the dramatic lifespan phenotypes that we observed in our experiments. The *myo2(LQ)* mutant shows a much stronger replicative lifespan phenotype than Δ*mmr1* and Δ*ypt11*, and the inability of the majority of cells to produce long-lived progeny correlates well with a strong mitochondrial inheritance defect. Thus, our results support the view that mitochondrial quantity, rather than quality, is affected by transport defects. We propose that inheritance of a critical mitochondrial quantity is an important factor determining yeast replicative lifespan.

Myo2-dependent mitochondrial transport determines the segregation of cytosolic protein aggregates. A role of Myo2 in aggregate retention was reported previously (Liu et al., 2010; Song et al., 2014; Hill et al., 2016). It was suggested that Myo2

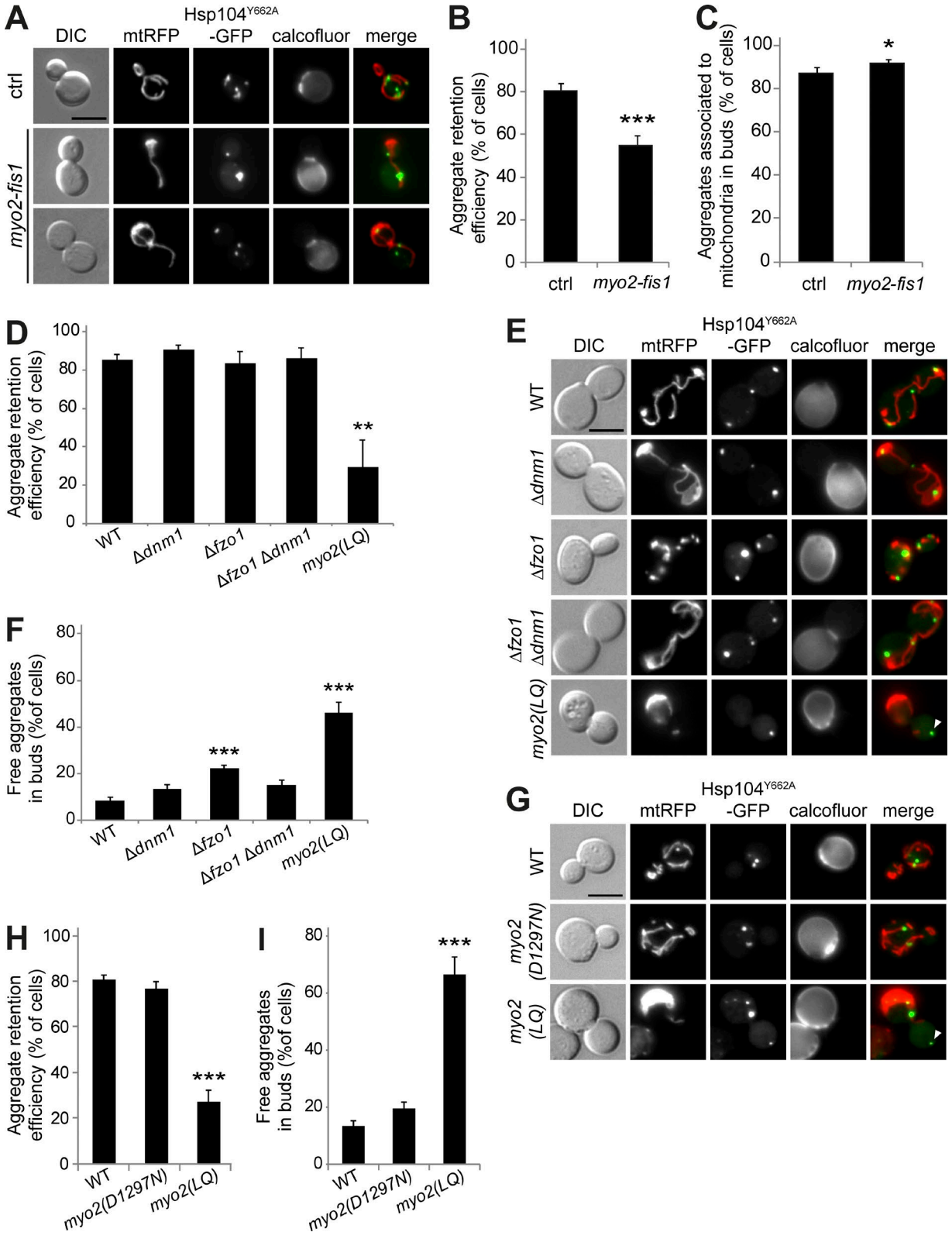

Figure 8. **Mitochondrial partitioning affects cytosolic protein aggregate retention.** (A) Cells expressing Hsp104^{Y662A}-GFP, mtRFP, and either Myo2-Fis1 from a multicopy plasmid or an empty vector control were grown at 30°C and stained with calcofluor. After applying a heat shock at 42°C for 5 min, cultures were incubated in the absence of calcofluor at 30°C for 2–3 h. Cells with medium-sized buds lacking calcofluor staining were analyzed by fluorescence microscopy. Bar, 5 µm. (B and C) Cells prepared as in A were scored for aggregate retention (i.e., aggregates were only present in the mother cell) or mitochondria-associated aggregates in buds. (D–I) Cells were analyzed as in A–C. Representative images of cells showing no aggregate retention are shown in E. Buds were quantified that showed no aggregate retention (i.e., one or more aggregates were visible in the bud; F) and contained aggregates that were not associated with mitochondria I. In G–I, Δ*myo2* cells expressed *MYO2* alleles from plasmids. Arrowheads indicate bud-localized aggregates that are not associated with mitochondria. Data pooling and statistics are detailed in Table S4.

is required for transport of vesicles that carry factors necessary for establishment of the polarisome at the bud tip, which then coordinates the retrograde flow of actin cables carrying associated protein aggregates away from the bud tip (Liu et al., 2010). In addition, Myo2 was proposed to contribute to the deposition of aggregated proteins at the IPOD (insoluble-protein-deposit) site at the vacuole (Hill et al., 2016). A possible role of mitochondria was not considered in these scenarios. Interestingly, the *myo2-14*, *myo2-16* (Schott et al., 1999), and *myo2-N1304S* (Pashkova et al., 2006) alleles used in these studies all carry mutations in the proximal half of the Myo2 cargo-binding domain, which is important for mitochondrial transport. Indeed, mitochondrial inheritance defects were demonstrated for *myo2-14* (Chernyakov et al., 2013) and *myo2-N1304S* (Altmann et al., 2008; Förtsch et al., 2011). Thus, it is possible that Myo2-dependent mitochondrial transport is more important for distribution of cytosolic protein aggregates than previously anticipated. Here, we report two lines of evidence suggesting that Myo2 plays an active and direct role in this process by controlling mitochondrial distribution. First, the aggregate retention defect of *myo2(LQ)* is not observed in the vacuole-specific mutant *myo2(D1297N)*. Second, enforcement of bud-directed transport by expression of the mitochondria-specific motor, Myo2-Fis1, results in increased partitioning of protein aggregates to the bud. Thus, both a loss-of-function and a gain-of-function allele of *MYO2* affect segregation of cytosolic protein aggregates in a mitochondria-dependent manner. Consistent with the tethering of aggregates to mitochondria observed by Zhou et al. (2014) and in this study (Fig. 8), we suggest that Myo2-dependent mitochondrial distribution is a key factor determining segregation of heat stress–induced cytosolic protein aggregates.

Coordination of fusion, fission, and transport presumably is important for mitochondrial distribution not only in yeast but also in higher organisms. Mitofusin 2 (Mfn2) is a human homologue of yeast Fzo1. Mutations cause Charcot–Marie–Tooth neuropathy type 2A, a disease characterized by degeneration of peripheral sensory and motor axons (Züchner et al., 2004). Interestingly, expression of disease-associated Mfn2 mutant proteins induces abnormal clustering of small fragmented mitochondria and impairs axonal transport of mitochondria in cultured dorsal root ganglion neurons (Baloh et al., 2007). Similarly, mutant Purkinje cells lacking Mfn2 contain clustered mitochondria in the cell body, and mitochondria fail to enter dendritic tracts (Chen et al., 2007). Furthermore, mammalian mitofusins were found to interact with Miro and Milton proteins, members of a receptor complex that links mitochondria to kinesin motor proteins in axonal transport (Misko et al., 2010). Thus, distribution of mitochondria in neurons depends on balanced fusion and fission dynamics, and fusion and transport activity appear to be coordinated. We hypothesize that a fine-tuned ratio of the transport rate and the size of the mitochondrial cargo is important for mitochondrial distribution in both yeast and neurons and possibly in other cell types. Evidence for asymmetric partitioning of cellular components, including mitochondria and protein aggregates, has also been reported for higher eukaryotic cells (Rujano et al., 2006; Ogrodnik et al., 2014; Katajisto et al., 2015; Moore and Jessberger, 2017). It will be interesting to see in the future whether the mechanisms that control asymmetric partitioning of mitochondria and protein aggregates in yeast are similar in mammals and contribute to cellular rejuvenation.

Materials and methods

Yeast strains

Yeast strains were isogenic to BY4741 or BY4742 (Brachmann et al., 1998). Deletion mutants were taken from the yeast deletion collection (Giaever et al., 2002) or constructed by homologous recombination using the *HIS3MX6* cassette (Wach et al., 1997). The query strain for SGA screening was constructed by PCR amplification of the 3′ part of the *myo2(LQ)* allele from plasmid pRS413-myo2(LQ) (Förtsch et al., 2011) using oligonucleotides 5′-CAGGTTATTGGAGGACAC-3′ and 5′-CTTTTTTTAGCATTCATGTACAATTTTGTTTCTCGCGCCATCAGTGCCGATTTCGGCCTATTGG-3′. The resulting PCR product was mixed with the a *URA3* marker amplified from plasmid pRS416 (Sikorski and Hieter, 1989) using oligonucleotides 5′-GAGCAGATTGTACTGAGAGTGC-3′ and 5′-CTTTTTTTAGCATTCATGTACAATTTTGTTTCTCGCGCCATCAGTTGCCGATTTCGGCCTATTGG-3′ and amplified in another round of PCR. The resulting *myo2(LQ) URA3* cassette was inserted by homologous recombination into the *MYO2* locus of yeast strain Y7092 (Tong and Boone, 2007) and confirmed by DNA sequencing. A WT control strain carried an analogous insertion of a *MYO2 URA3* cassette. The *hsp104^{Y662A}-GFP* allele together with a *HIS3* marker was amplified by PCR from genomic DNA of strain RLY7200 (Zhou et al., 2011) using oligonucleotides 5′-AAACCTTCTGCACCATTTTTA-3′ and 5′-GCAAGATGAACTAAACGTTAA-3′ and inserted by homologous recombination into the *HSP104* locus of recipient strains. To make the *HIS3* marker available in some *hsp104^{Y662A}-GFP* strains, the *HIS3* cassette of RLY7200 (Zhou et al., 2011) was replaced by homologous recombination with a *natNT2* cassette amplified from plasmid pYM-N7 (Janke et al., 2004) using oligonucleotides 5′-GACATGGAGGCCCAGAATAC-3′ and 5′-CTTGAAAACAAGAATCTTTTTATTGTCAGTATCCTTCGATTACAACAGGTGTTGTCC-3′. Yeast strains are listed in Table S3.

Growth and manipulation of yeast

Growth and manipulation of yeast strains was performed according to standard procedures (Sherman, 1991; Gietz et al., 1992). To induce loss of mtDNA, cells were incubated overnight at 30°C under agitation in 1 ml YPD medium containing 50 µg/ml ethidium bromide. Then, cells were spread on YPD plates and incubated for 2 d at 30°C. Loss of mtDNA in single colonies was confirmed by lack of growth on YPG plates and DAPI staining. 5-FOA was added to plates at a concentration of 1 mg/ml, and doxycycline was added to plates and liquid medium at concentrations of 10 µg/ml and 4 µg/ml, respectively. Tetrad dissection and replicative lifespan analysis were performed with a Singer MSM Series 300 micromanipulator equipped with an Acer n30 pocket PC (Singer Instruments). Sizes of colonies generated by tetrad dissection were determined with ImageJ software version 1.43 (Schneider et al., 2012) after conversion of photographs of agar plates to binary pictures. For lifespan analysis (Park et al., 2002), cells were first grown on YPG plates to select for respiratory active cells and then transferred to YPD plates. After 5 h at 30°C, single cells were picked and arrayed on the plate. After the first cell division, the mother cell was discarded and the virgin cells were monitored for newly formed daughters. Daughter cells were counted and removed until the mother cell ceased to produce new buds. Plates were kept at 30°C during the day and stored at 4°C at night. The analysis of productively reproducing juvenile cells was performed identically with two exceptions: (1) cells were grown on selection medium (synthetic complete dextrose medium [SCD], lacking leucine) during all stages of the analysis, and (2) newly formed daughter cells were not removed from virgin cells. Instead, the ability to reproduce was assayed by scoring the frequency of (micro)colony formation after an incubation at 30°C for 3 d.

SGA screening

SGA was performed using a ROTOR HDA robot (Singer Instruments) essentially as described previously (Baryshnikova et al., 2010). Query strains were incubated on YPD medium for 2 d at 30°C. The *MAT*a deletion library (Giaever et al., 2002) was plated in a 384 format on YPD, incubated for 2 to 3 d at room temperature, and then arrayed to a high-density 1,536 format on YPD. Each deletion strain was present in four replicates. The query strains were mixed with this high-density array and allowed to mate for one day at room temperature. Colonies were then plated on diploid selection medium (SCD [monosodium glutamic acid] containing 200 mg/l G418, but lacking uracil) and grown for 1 d at 30°C. This selection was repeated once before cells were plated on enriched sporulation medium and incubated at 22°C for 5 to 10 d. For haploid selection, yeast cells were plated on *MAT*a selection medium (SCD lacking histidine, arginine, lysine; containing 50 mg/l canavanine, 50 mg/l thialysine), incubated for 2 d at 30°C, and then plated on *MAT*a/*kanR* selection medium (SCD [monosodium gluatmic acid] lacking histidine, arginine, lysine; containing 50 mg/l canavanine, 50 mg/l thialysine, and 200 mg/l G418) and incubated for 1 d at 30°C. Cells were then replica-plated on *MAT*a/*kanR*/*URA3* selection medium (SCD [monosodium gluatmic acid] lacking histidine, arginine, lysine, uracil; containing 50 mg/l canavanine, 50 mg/l thialysine, and 200 mg/l G418) and incubated for 1 to 2 d until colonies grew to a substantial size. This step was repeated once. Finally, colonies were replica-plated once more on *MAT*a/*kanR*/*URA3* selection medium and incubated for 20 h at 30°C. Photographs of the plates were taken using a Kodak EasyShare DX7590 camera. Genetic interactors were identified by visual inspection or using SGAtools software (Wagih et al., 2013). Strains with a genetic interaction score below −0.3 were considered synthetic sick. The SGA screen was performed twice and only strains reproducibly found in both screens were considered as bona fide interactors.

GO term analysis

Functional enrichment analysis of GO terms was performed using the GO term finder tool at the Saccharomyces Genome Database (Boyle et al., 2004; Cherry et al., 2012). The list of negative interactors was uploaded together with the background set of screened strains, functional enrichments of GO terms for processes with a p-value < 0.05 were searched, and the ratio of the cluster frequency and the background frequency was determined.

Plasmids

Plasmids pRS413-MYO2 (Catlett and Weisman, 1998), pRS413-myo2(LQ) (Förtsch et al., 2011), and pRS413-D1297N (Catlett et al., 2000) were described previously. Plasmid pAG415GPD-YPT11 for overexpression of Ypt11 was constructed by PCR amplification of the *YPT11* ORF from genomic DNA using oligonucleotides 5′-GGGGACAAGTTTGTACAAAAAAGCAGGCTTCATGTCCCA GAGAAAGCGATAC-3′ and 5′-GGGGACCACTTTGTACAAGAA AGCTGGGTCCGAATCTTGTTGTATAATTTGTCG-3′ and cloning into pAG415GPD-ccdB by Gateway cloning (Alberti et al., 2007). Plasmid pAG415GPD-ypt11(G40D) for overexpression of inactive Ypt11(G40D) was constructed using the same strategy and plasmid pSA214 (Arai et al., 2008) as a template. Plasmids pRS316-myo2-fis1 and pRS426-myo2-fis1 for expression of Myo2-Fis1 from the *MYO2* promoter were described before (Förtsch et al., 2011). Plasmids for inducible expression of Myo2-Fis1, pAG423GAL-myo2-fis1 and pVV209-myo2-fis1, were constructed by Gateway cloning using the same strategy as described before (Klecker et al., 2013) using vectors pAG423GAL-ccdB (Alberti et al., 2007) and pVV209 (Van Mullem et al., 2003). Plasmid pRS416-FZO1 (Fritz et al., 2001) containing *FZO1* with its own regulatory sequences and a *URA3* marker was used for plasmid shuffling. Plasmids for expression of *FZO1* and *fzo1-1*, pRS313-FZO1, and pRS313-fzo1-1 were constructed by PCR amplification of the alleles, including endogenous promoter and terminator sequences from genomic DNA of *FZO1* or *fzo1-1* strains (Hermann et al., 1998) using oligonucleotides 5′-TTTTCTAGAGTGCTTGAGTATCAGGAG AAGG-3′ and 5′-TTTGAATTCGAGCTATTACTTCCAGGGAC-3′ and cloned into the XbaI/EcoRI sites of pRS313 (Sikorski and Hieter, 1989). Plasmids pYES-mtGFP, pYX122-mtGFP, pYX142-mtGFP (Westermann and Neupert, 2000), pMitoLoc (Vowinckel et al., 2015), and pYX142-mtERFP (Scholz et al., 2013) for mitochondrial staining were described previously. pYES-mtERFP for expression of mitochondria-targeted RFP (mtRFP) was constructed by PCR amplification of *yEmRFP* from plasmid yEpGAP-Cherry (Keppler-Ross et al., 2008) using oligonucleotides 5′-TATATAAGATCTGTTTCAAAAGGTGAA GAAGATAATA-3′ and 5′-TATATACTCGAGTTATTTATATAATTC-3′ and cloned into the BglII and XhoI sites of pYES-mtGFP.

Staining of cellular structures and protein aggregates

If not indicated otherwise, cells were grown in glucose-containing medium and analyzed at the logarithmic growth phase. Mitochondria were stained by expression of mtGFP or mtRFP from plasmids (see previous paragraph). Staining of vacuoles with CellTracker Blue CMAC was performed as described previously (Böckler and Westermann, 2014). For quantifications of organelle inheritance phenotypes, cells were incubated at 30°C (if not indicated otherwise), and organelles transported to small- and medium-sized buds were scored in live or fixed cells. For staining of DNA, cells were fixed with 100% methanol for 5 min, washed once with PBS, and resuspended in PBS. 1 µg/ml DAPI was added, and cells were incubated for 5 min at room temperature. Cells were washed four times and resuspended in PBS before fluorescence microscopy. For cell wall staining, cells were washed and resuspended in 10 mM Hepes, 2% glucose, pH 7.2, and stained with 25 µM calcofluor for 30 min under agitation. Cells were washed with buffer before they were resuspended in fresh medium and further incubated. For staining of heat stress–induced cytosolic protein aggregates, cells expressing $Hsp104^{Y662A}$-GFP (Zhou et al., 2011) were grown to mid-log phase and stained with calcofluor. Heat shock was performed for 5 min at 42°C under agitation. The cells were then further cultivated to allow bud formation and fixed in 3.7% formaldehyde before microscopy. Growth and staining were performed at 30°C with the exception of temperature-sensitive mutants and their control strains, which were incubated at 25°C.

Microscopy

Epifluorescence microscopy was performed using an Axioplan 2 microscope (ZEISS) equipped with a Plan Neofluar 100×/1.30 Ph3 oil objective and an Evolution VF Mono Cooled monochrome camera (Intas) with Image ProPlus 5.0 and Scope Pro4.5 software (Media Cybernetics) or QCapture Pro 6 software (QImaging) or an Axiophot microscope (ZEISS) equipped with a Plan Neofluar 100×/1.30 Ph3 oil objective and a DCF360FX Camera (Leica Biosystems) with LAF AF Version 2.2.1 Software (Leica Biosystems). Time-resolved 3D fluorescence microscopy was performed as described previously (Scholz et al., 2013) using a CellASIC Onix Microfluidic Perfusion System (CellASIC Corp.), ONIX Microfluidic Plates (Y04C Yeast Perfusion Plate, 3.5–5 µm) and ONIX FG Software on a DMI 6000 wide field fluorescence microscope (Leica Biosystems) equipped with an HCX PL APO 100×/1.40–0.70 oil objective, DFC360FX camera (high-speed kit; Leica Biosystems), an incubator BL (PeCon GmbH), and LAS AF Software Version 2.1.0. Image manipulations other than minor adjustments of brightness and contrast were not performed.

Statistics

For statistical analysis, SigmaPlot V13 (Systat Software) was used. For comparing two groups, unpaired two-tailed Student's *t* tests with ad hoc normality (Shapiro–Wilk) and equal variance (Browne–Forsythe) tests were applied. If ad hoc tests failed, Mann–Whitney rank sum test was used. For all other comparisons one-way analysis of variance with ad hoc normality (Shapiro–Wilk) and equal variance (Browne–Forsythe) tests and Holm–Sidak as post hoc test were applied. If ad hoc tests failed, Kruskal–Wallis one-way analysis of variance on ranks was used with Dunn as post hoc test. Differences were considered to be significant with p-values < 0.05 (*, $P < 0.05$; **, $P < 0.01$; and ***, $P < 0.001$). If not indicated otherwise, significance was compared with WT values. Error bars indicate standard deviation. If not indicated otherwise, three independent experiments with at least 100 cells per experiment were analyzed. Data pooling and statistics for each experiment is detailed in Table S4.

Model and simulations

A one-dimensional model was constructed that considers the long axis between a mother yeast cell and a single daughter cell, both having fixed diameters of 5 µm. The total system length (L = 10 µm) was divided into lattice sites of size $\Delta x = 50$ nm so that individual mitochondrial particles (length of 550 nm) occupied $n = 11$ sites on the lattice. In all cases, a total amount of $n = 38$ mitochondrial particles were considered that needed to be distributed between mother (positions $x < 5$ µm) and daughter (positions $x > 5$ µm) within a period of 2 h. For the fusion-deficient scenario, we considered dispersed individual particles whereas two linear chains (each consisting of 19 particles) were used to model the WT situation. In both scenarios, two mitochondrial particles were assumed to be anchored via Num1 to the mother's plasma membrane ($x = 0$), i.e., these two mitochondrial particles were not moved throughout the simulation. Remaining mitochondrial particles were allowed to diffuse with a diffusion constant $D = 10^{-3}$ µm²/s; active anterograde transport into daughter cells along actin filaments and retrograde transport (e.g., caused by backflow of actin filaments) were assigned velocities $v_a = v_r = 0.4$ µm/s. Particle dynamics was implemented by a Monte Carlo scheme: Within each time step ($\Delta t = 0.1$ s), a total number of N-2 mitochondrial particles were picked at random and tested for a potential move to nearest-neighbor lattice sites. The total probability for a jump was given by the sum of probabilities to move to the left and right, $P = p_{left} + p_{right}$. Individual jump probabilities were $p_{left} = D\Delta t/\Delta x^2 + (1 - a)v_r\Delta t$ and $p_{right} = D\Delta t/\Delta x^2 + av_a\Delta t$ with $a = 1$ when the particle was attached to actin filaments (otherwise, $a = 0$). Depending on additional constraints (mitochondrial network formation or a maximum occupation number per site), the individual jump probabilities were set to zero.

Individual mitochondrial particles were allowed to attach to actin for anterograde transport with rate $k_{on} = 0.005$/s, the corresponding dissociation rate was varied in a range $0.01/s \leq k_{off} \leq 0.12/s$. Mitochondrial particles that were part of a network structure were assigned an enhanced association rate $k_{on} = 0.025$/s or $k_{on} = 0.125$/s when one or both next neighbors in the network were already associated with actin. This choice considers the reduced freedom of individual mitochondria to leave the vicinity of actin filaments when being part of a mitochondrial network and hence is a reflection of collective effects.

To mimic mitochondrial networks in WT cells, we assumed all mitochondrial particles to be part of two polymeric tubules, i.e., each tubule contained a linear sequence of N/2 mitochondrial particles. In each tubule, one end particle was assumed to be Num1-anchored and therefore remained at a fixed position $x = 0$. All other particles within a tubule were demanded to stay in touch with their next neighbors regardless of the jump probabilities p_{left} and p_{right}, i.e., any move leading to a loss of contact between particle "i" and its neighbors "i − 1" and "I + 1" was blocked. By this constraint, the polymeric tube stayed intact and was able to assume coil-like and even fully stretched configurations. In addition, a maximum site occupancy could be imposed that served as a simple means to consider the varying volume elements of the spherical cells along the one-dimensional axis. If a site had reached its maximum occupancy, no additional mitochondrial particle was allowed to move to that site and the corresponding jump probability was set to zero. For data shown in Fig. 5 we imposed a roughly parabolic variation of the maximum occupancy, calculated via the volume of a spherical cap of thickness h, $V = \pi h^2 (R - h/3)$, with 12 particles in each cell's middle and at least four particles near the cell poles and in the bud neck.

To arrive at significant results despite the small number of mitochondrial particles, we performed 200 simulations for each parameter condition and used these data to obtain the mean number of mitochondrial particles at each lattice site over time. The final quantity fraction of mitochondria in the daughter was determined from this by integrating over the range $x > 5$ µm at the end of the temporal evolution.

Online supplemental material

Tables S1–S4 are available as Excel files. Table S1 lists genes and genetic interaction scores from two independent SGA screens of the *MAT*a yeast deletion collection with *myo2(LQ)*. Table S2 lists genes that negatively interacted with *myo2(LQ)* in SGA screens. Table S3 lists yeast strains used in this study. Table S4 details data pooling and statistics. Video 1 shows mitochondrial movements in WT cells at 37°C. Video 2 shows mitochondrial movements in *fzo1-1* cells at 37°C. Video 3 shows mitochondrial movements in *myo2(LQ)* cells at 37°C. Video 4 shows mitochondrial movements in *myo2(LQ) fzo1-1* cells at 37°C. Video 5 shows mitochondrial movements in WT cells at 30°C. Video 6 shows mitochondrial movements in Δ*mmr1* cells at 30°C. Video 7 shows mitochondrial movements in Δ*fzo1* cells at 30°C. Video 8 shows mitochondrial movements in Δ*fzo1* Δ*mmr1* cells at 30°C.

Acknowledgments

We are grateful to the Westermann laboratory for helpful discussions and to Charles Boone and Rong Li for making plasmids and yeast strains available to us.

This work was supported by Deutsche Forschungsgemeinschaft through grant WE 2174/5-2 and by Elitenetzwerk Bayern through the "Biological Physics" program.

The authors declare no competing financial interests.

Author contributions: S. Böckler and B. Westermann conceived and designed the study; S. Böckler, N. Hock, X. Chelius, T. Klecker, and M. Wolter designed, performed, and interpreted experiments; M. Weiss conceived and conducted the simulations; all authors analyzed the data; and B. Westermann wrote the manuscript with input from all authors.

Submitted: 30 November 2016
Revised: 13 April 2017
Accepted: 12 May 2017

References

Alberti, S., A.D. Gitler, and S. Lindquist. 2007. A suite of Gateway cloning vectors for high-throughput genetic analysis in *Saccharomyces cerevisiae. Yeast.* 24:913–919. http://dx.doi.org/10.1002/yea.1502

Altmann, K., M. Frank, D. Neumann, S. Jakobs, and B. Westermann. 2008. The class V myosin motor protein, Myo2, plays a major role in mitochondrial motility in *Saccharomyces cerevisiae. J. Cell Biol.* 181:119–130. http://dx.doi.org/10.1083/jcb.200709099

Arai, S., Y. Noda, S. Kainuma, I. Wada, and K. Yoda. 2008. Ypt11 functions in bud-directed transport of the Golgi by linking Myo2 to the coatomer

subunit Ret2. *Curr. Biol.* 18:987–991. http://dx.doi.org/10.1016/j.cub.2008.06.028

Baloh, R.H., R.E. Schmidt, A. Pestronk, and J. Milbrandt. 2007. Altered axonal mitochondrial transport in the pathogenesis of Charcot–Marie–Tooth disease from mitofusin 2 mutations. *J. Neurosci.* 27:422–430. http://dx.doi.org/10.1523/JNEUROSCI.4798-06.2007

Baryshnikova, A., M. Costanzo, S. Dixon, F.J. Vizeacoumar, C.L. Myers, B. Andrews, and C. Boone. 2010. Synthetic genetic array (SGA) analysis in *Saccharomyces cerevisiae* and *Schizosaccharomyces pombe. Methods Enzymol.* 470:145–179. http://dx.doi.org/10.1016/S0076-6879(10)70007-0

Bleazard, W., J.M. McCaffery, E.J. King, S. Bale, A. Mozdy, Q. Tieu, J. Nunnari, and J.M. Shaw. 1999. The dynamin-related GTPase Dnm1 regulates mitochondrial fission in yeast. *Nat. Cell Biol.* 1:298–304. http://dx.doi.org/10.1038/13014

Böckler, S., and B. Westermann. 2014. Mitochondrial ER contacts are crucial for mitophagy in yeast. *Dev. Cell.* 28:450–458. http://dx.doi.org/10.1016/j.devcel.2014.01.012

Boyle, E.I., S. Weng, J. Gollub, H. Jin, D. Botstein, J.M. Cherry, and G. Sherlock. 2004. GO:TermFinder—Open source software for accessing Gene Ontology information and finding significantly enriched Gene Ontology terms associated with a list of genes. *Bioinformatics.* 20:3710–3715. http://dx.doi.org/10.1093/bioinformatics/bth456

Brachmann, C.B., A. Davies, G.J. Cost, E. Caputo, J. Li, P. Hieter, and J.D. Boeke. 1998. Designer deletion strains derived from *Saccharomyces cerevisiae* S288C: A useful set of strains and plasmids for PCR-mediated gene disruption and other applications. *Yeast.* 14:115–132. http://dx.doi.org/10.1002/(SICI)1097-0061(19980130)14:2<115::AID-YEA204>3.0.CO;2-2

Burgess, S.M., M. Delannoy, and R.E. Jensen. 1994. *MMM1* encodes a mitochondrial outer membrane protein essential for establishing and maintaining the structure of yeast mitochondria. *J. Cell Biol.* 126:1375–1391. http://dx.doi.org/10.1083/jcb.126.6.1375

Catlett, N.L., and L.S. Weisman. 1998. The terminal tail region of a yeast myosin-V mediates its attachment to vacuole membranes and sites of polarized growth. *Proc. Natl. Acad. Sci. USA.* 95:14799–14804. http://dx.doi.org/10.1073/pnas.95.25.14799

Catlett, N.L., J.E. Duex, F. Tang, and L.S. Weisman. 2000. Two distinct regions in a yeast myosin-V tail domain are required for the movement of different cargoes. *J. Cell Biol.* 150:513–526. http://dx.doi.org/10.1083/jcb.150.3.513

Chen, H., J.M. McCaffery, and D.C. Chan. 2007. Mitochondrial fusion protects against neurodegeneration in the cerebellum. *Cell.* 130:548–562. http://dx.doi.org/10.1016/j.cell.2007.06.026

Chernyakov, I., F. Santiago-Tirado, and A. Bretscher. 2013. Active segregation of yeast mitochondria by Myo2 is essential and mediated by Mmr1 and Ypt11. *Curr. Biol.* 23:1818–1824. http://dx.doi.org/10.1016/j.cub.2013.07.053

Cherry, J.M., E.L. Hong, C. Amundsen, R. Balakrishnan, G. Binkley, E.T. Chan, K.R. Christie, M.C. Costanzo, S.S. Dwight, S.R. Engel, et al. 2012. Saccharomyces Genome Database: The genomics resource of budding yeast. *Nucleic Acids Res.* 40(D1):D700–D705. http://dx.doi.org/10.1093/nar/gkr1029

Erjavec, N., L. Larsson, J. Grantham, and T. Nyström. 2007. Accelerated aging and failure to segregate damaged proteins in Sir2 mutants can be suppressed by overproducing the protein aggregation-remodeling factor Hsp104p. *Genes Dev.* 21:2410–2421. http://dx.doi.org/10.1101/gad.439307

Eves, P.T., Y. Jin, M. Brunner, and L.S. Weisman. 2012. Overlap of cargo binding sites on myosin V coordinates the inheritance of diverse cargoes. *J. Cell Biol.* 198:69–85. http://dx.doi.org/10.1083/jcb.201201024

Farkasovsky, M., and H. Küntzel. 1995. Yeast Num1p associates with the mother cell cortex during S/G2 phase and affects microtubular functions. *J. Cell Biol.* 131:1003–1014. http://dx.doi.org/10.1083/jcb.131.4.1003

Fehrenbacher, K.L., H.C. Yang, A.C. Gay, T.M. Huckaba, and L.A. Pon. 2004. Live cell imaging of mitochondrial movement along actin cables in budding yeast. *Curr. Biol.* 14:1996–2004. http://dx.doi.org/10.1016/j.cub.2004.11.004

Förtsch, J., E. Hummel, M. Krist, and B. Westermann. 2011. The myosin-related motor protein Myo2 is an essential mediator of bud-directed mitochondrial movement in yeast. *J. Cell Biol.* 194:473–488. http://dx.doi.org/10.1083/jcb.201012088

Frederick, R.L., J.M. McCaffery, K.W. Cunningham, K. Okamoto, and J.M. Shaw. 2004. Yeast Miro GTPase, Gem1p, regulates mitochondrial morphology via a novel pathway. *J. Cell Biol.* 167:87–98. http://dx.doi.org/10.1083/jcb.200405100

Fritz, S., D. Rapaport, E. Klanner, W. Neupert, and B. Westermann. 2001. Connection of the mitochondrial outer and inner membranes by Fzo1 is critical for organellar fusion. *J. Cell Biol.* 152:683–692. http://dx.doi.org/10.1083/jcb.152.4.683

Giaever, G., A.M. Chu, L. Ni, C. Connelly, L. Riles, S. Véronneau, S. Dow, A. Lucau-Danila, K. Anderson, B. André, et al. 2002. Functional profiling of the *Saccharomyces cerevisiae* genome. *Nature.* 418:387–391. http://dx.doi.org/10.1038/nature00935

Gietz, D., A. St Jean, R.A. Woods, and R.H. Schiestl. 1992. Improved method for high efficiency transformation of intact yeast cells. *Nucleic Acids Res.* 20:1425. http://dx.doi.org/10.1093/nar/20.6.1425

Goldring, E.S., L.I. Grossman, D. Krupnick, D.R. Cryer, and J. Marmur. 1970. The petite mutation in yeast. Loss of mitochondrial deoxyribonucleic acid during induction of petites with ethidium bromide. *J. Mol. Biol.* 52:323–335. http://dx.doi.org/10.1016/0022-2836(70)90033-1

Henderson, K.A., and D.E. Gottschling. 2008. A mother's sacrifice: What is she keeping for herself? *Curr. Opin. Cell Biol.* 20:723–728. http://dx.doi.org/10.1016/j.ceb.2008.09.004

Hermann, G.J., J.W. Thatcher, J.P. Mills, K.G. Hales, M.T. Fuller, J. Nunnari, and J.M. Shaw. 1998. Mitochondrial fusion in yeast requires the transmembrane GTPase Fzo1p. *J. Cell Biol.* 143:359–373. http://dx.doi.org/10.1083/jcb.143.2.359

Higuchi-Sanabria, R., W.M. Pernice, J.D. Vevea, D.M. Alessi Wolken, I.R. Boldogh, and L.A. Pon. 2014. Role of asymmetric cell division in lifespan control in *Saccharomyces cerevisiae. FEMS Yeast Res.* 14:1133–1146. http://dx.doi.org/10.1111/1567-1364.12216

Higuchi-Sanabria, R., J.K. Charalel, M.P. Viana, E.J. Garcia, C.N. Sing, A. Koenigsberg, T.C. Swayne, J.D. Vevea, I.R. Boldogh, S.M. Rafelski, and L.A. Pon. 2016. Mitochondrial anchorage and fusion contribute to mitochondrial inheritance and quality control in the budding yeast *Saccharomyces cerevisiae. Mol. Biol. Cell.* 27:776–787. http://dx.doi.org/10.1091/mbc.E15-07-0455

Hill, S.M., X. Hao, J. Grönvall, S. Spikings-Nordby, P.O. Widlund, T. Amen, A. Jörhov, R. Josefson, D. Kaganovich, B. Liu, and T. Nyström. 2016. Asymmetric inheritance of aggregated proteins and age reset in yeast are regulated by Vac17-dependent vacuolar functions. *Cell Reports.* 16:826–838. http://dx.doi.org/10.1016/j.celrep.2016.06.016

Hughes, A.L., and D.E. Gottschling. 2012. An early age increase in vacuolar pH limits mitochondrial function and lifespan in yeast. *Nature.* 492:261–265. http://dx.doi.org/10.1038/nature11654

Hwang, E., J. Kusch, Y. Barral, and T.C. Huffaker. 2003. Spindle orientation in *Saccharomyces cerevisiae* depends on the transport of microtubule ends along polarized actin cables. *J. Cell Biol.* 161:483–488. http://dx.doi.org/10.1083/jcb.200302030

Itoh, T., A. Watabe, A. Toh-E, and Y. Matsui. 2002. Complex formation with Ypt11p, a rab-type small GTPase, is essential to facilitate the function of Myo2p, a class V myosin, in mitochondrial distribution in *Saccharomyces cerevisiae. Mol. Cell. Biol.* 22:7744–7757. http://dx.doi.org/10.1128/MCB.22.22.7744-7757.2002

Itoh, T., A. Toh-E, and Y. Matsui. 2004. Mmr1p is a mitochondrial factor for Myo2p-dependent inheritance of mitochondria in the budding yeast. *EMBO J.* 23:2520–2530. http://dx.doi.org/10.1038/sj.emboj.7600271

Janke, C., M.M. Magiera, N. Rathfelder, C. Taxis, S. Reber, H. Maekawa, A. Moreno-Borchart, G. Doenges, E. Schwob, E. Schiebel, and M. Knop. 2004. A versatile toolbox for PCR-based tagging of yeast genes: new fluorescent proteins, more markers and promoter substitution cassettes. *Yeast.* 21:947–962. http://dx.doi.org/10.1002/yea.1142

Kaeberlein, M., M. McVey, and L. Guarente. 1999. The SIR2/3/4 complex and SIR2 alone promote longevity in *Saccharomyces cerevisiae* by two different mechanisms. *Genes Dev.* 13:2570–2580. http://dx.doi.org/10.1101/gad.13.19.2570

Katajisto, P., J. Döhla, C.L. Chaffer, N. Pentinmikko, N. Marjanovic, S. Iqbal, R. Zoncu, W. Chen, R.A. Weinberg, and D.M. Sabatini. 2015. Stem cells. Asymmetric apportioning of aged mitochondria between daughter cells is required for stemness. *Science.* 348:340–343. http://dx.doi.org/10.1126/science.1260384

Keppler-Ross, S., C. Noffz, and N. Dean. 2008. A new purple fluorescent color marker for genetic studies in *Saccharomyces cerevisiae* and *Candida albicans*. *Genetics.* 179:705–710. http://dx.doi.org/10.1534/genetics.108.087080

Klecker, T., D. Scholz, J. Förtsch, and B. Westermann. 2013. The yeast cell cortical protein Num1 integrates mitochondrial dynamics into cellular architecture. *J. Cell Sci.* 126:2924–2930. http://dx.doi.org/10.1242/jcs.126045

Knoblach, B., and R.A. Rachubinski. 2015. Sharing the cell's bounty: Organelle inheritance in yeast. *J. Cell Sci.* 128:621–630. http://dx.doi.org/10.1242/jcs.151423

Lackner, L.L., H. Ping, M. Graef, A. Murley, and J. Nunnari. 2013. Endoplasmic reticulum-associated mitochondria-cortex tether functions in the

distribution and inheritance of mitochondria. *Proc. Natl. Acad. Sci. USA.* 110:E458–E467. http://dx.doi.org/10.1073/pnas.1215232110

Lewandowska, A., J. Macfarlane, and J.M. Shaw. 2013. Mitochondrial association, protein phosphorylation, and degradation regulate the availability of the active Rab GTPase Ypt11 for mitochondrial inheritance. *Mol. Biol. Cell.* 24:1185–1195. http://dx.doi.org/10.1091/mbc.E12-12-0848

Liu, B., L. Larsson, A. Caballero, X. Hao, D. Öling, J. Grantham, and T. Nyström. 2010. The polarisome is required for segregation and retrograde transport of protein aggregates. *Cell.* 140:257–267. http://dx.doi.org/10.1016/j.cell.2009.12.031

Liu, B., L. Larsson, V. Franssens, X. Hao, S.M. Hill, V. Andersson, D. Höglund, J. Song, X. Yang, D. Öling, et al. 2011. Segregation of protein aggregates involves actin and the polarity machinery. *Cell.* 147:959–961. http://dx.doi.org/10.1016/j.cell.2011.11.018

Longo, V.D., G.S. Shadel, M. Kaeberlein, and B. Kennedy. 2012. Replicative and chronological aging in *Saccharomyces cerevisiae. Cell Metab.* 16:18–31. http://dx.doi.org/10.1016/j.cmet.2012.06.002

Lum, R., J.M. Tkach, E. Vierling, and J.R. Glover. 2004. Evidence for an unfolding/threading mechanism for protein disaggregation by *Saccharomyces cerevisiae* Hsp104. *J. Biol. Chem.* 279:29139–29146. http://dx.doi.org/10.1074/jbc.M403777200

Matsui, Y. 2003. Polarized distribution of intracellular components by class V myosins in *Saccharomyces cerevisiae. Int. Rev. Cytol.* 229:1–42. http://dx.doi.org/10.1016/S0074-7696(03)29001-X

McFaline-Figueroa, J.R., J. Vevea, T.C. Swayne, C. Zhou, C. Liu, G. Leung, I.R. Boldogh, and L.A. Pon. 2011. Mitochondrial quality control during inheritance is associated with lifespan and mother-daughter age asymmetry in budding yeast. *Aging Cell.* 10:885–895. http://dx.doi.org/10.1111/j.1474-9726.2011.00731.x

Miller, S.B., C.T. Ho, J. Winkler, M. Khokhrina, A. Neuner, M.Y. Mohamed, D.L. Guilbride, K. Richter, M. Lisby, E. Schiebel, et al. 2015a. Compartment-specific aggregases direct distinct nuclear and cytoplasmic aggregate deposition. *EMBO J.* 34:778–797. http://dx.doi.org/10.15252/embj.201489524

Miller, S.B., A. Mogk, and B. Bukau. 2015b. Spatially organized aggregation of misfolded proteins as cellular stress defense strategy. *J. Mol. Biol.* 427:1564–1574. http://dx.doi.org/10.1016/j.jmb.2015.02.006

Misko, A., S. Jiang, I. Wegorzewska, J. Milbrandt, and R.H. Baloh. 2010. Mitofusin 2 is necessary for transport of axonal mitochondria and interacts with the Miro/Milton complex. *J. Neurosci.* 30:4232–4240. http://dx.doi.org/10.1523/JNEUROSCI.6248-09.2010

Moore, D.L., and S. Jessberger. 2017. Creating age asymmetry: Consequences of inheriting damaged goods in mammalian cells. *Trends Cell Biol.* 27:82–92. http://dx.doi.org/10.1016/j.tcb.2016.09.007

Mortimer, R.K., and J.R. Johnston. 1959. Life span of individual yeast cells. *Nature.* 183:1751–1752. http://dx.doi.org/10.1038/1831751a0

Nyström, T., and B. Liu. 2014. The mystery of aging and rejuvenation: A budding topic. *Curr. Opin. Microbiol.* 18:61–67. http://dx.doi.org/10.1016/j.mib.2014.02.003

Ogrodnik, M., H. Salmonowicz, R. Brown, J. Turkowska, W. Średniawa, S. Pattabiraman, T. Amen, A.C. Abraham, N. Eichler, R. Lyakhovetsky, and D. Kaganovich. 2014. Dynamic JUNQ inclusion bodies are asymmetrically inherited in mammalian cell lines through the asymmetric partitioning of vimentin. *Proc. Natl. Acad. Sci. USA.* 111:8049–8054. http://dx.doi.org/10.1073/pnas.1324035111

Otsuga, D., B.R. Keegan, E. Brisch, J.W. Thatcher, G.J. Hermann, W. Bleazard, and J.M. Shaw. 1998. The dynamin-related GTPase, Dnm1p, controls mitochondrial morphology in yeast. *J. Cell Biol.* 143:333–349. http://dx.doi.org/10.1083/jcb.143.2.333

Ouellet, J., and Y. Barral. 2012. Organelle segregation during mitosis: Lessons from asymmetrically dividing cells. *J. Cell Biol.* 196:305–313. http://dx.doi.org/10.1083/jcb.201102078

Park, P.U., M. McVey, and L. Guarente. 2002. Separation of mother and daughter cells. *Methods Enzymol.* 351:468–477. http://dx.doi.org/10.1016/S0076-6879(02)51865-6

Pashkova, N., Y. Jin, S. Ramaswamy, and L.S. Weisman. 2006. Structural basis for myosin V discrimination between distinct cargoes. *EMBO J.* 25:693–700. http://dx.doi.org/10.1038/sj.emboj.7600965

Pernice, W.M., J.D. Vevea, and L.A. Pon. 2016. A role for Mfb1p in region-specific anchorage of high-functioning mitochondria and lifespan in *Saccharomyces cerevisiae. Nat. Commun.* 7:10595. http://dx.doi.org/10.1038/ncomms10595

Ping, H.A., L.M. Kraft, W. Chen, A.E. Nilles, and L.L. Lackner. 2016. Num1 anchors mitochondria to the plasma membrane via two domains with different lipid binding specificities. *J. Cell Biol.* 213:513–524. http://dx.doi.org/10.1083/jcb.201511021

Pruyne, D., A. Legesse-Miller, L. Gao, Y. Dong, and A. Bretscher. 2004. Mechanisms of polarized growth and organelle segregation in yeast. *Annu. Rev. Cell Dev. Biol.* 20:559–591. http://dx.doi.org/10.1146/annurev.cellbio.20.010403.103108

Rafelski, S.M., M.P. Viana, Y. Zhang, Y.H. Chan, K.S. Thorn, P. Yam, J.C. Fung, H. Li, L.F. Costa, and W.F. Marshall. 2012. Mitochondrial network size scaling in budding yeast. *Science.* 338:822–824. http://dx.doi.org/10.1126/science.1225720

Rapaport, D., M. Brunner, W. Neupert, and B. Westermann. 1998. Fzo1p is a mitochondrial outer membrane protein essential for the biogenesis of functional mitochondria in *Saccharomyces cerevisiae. J. Biol. Chem.* 273:20150–20155. http://dx.doi.org/10.1074/jbc.273.32.20150

Roeder, A.D., G.J. Hermann, B.R. Keegan, S.A. Thatcher, and J.M. Shaw. 1998. Mitochondrial inheritance is delayed in *Saccharomyces cerevisiae* cells lacking the serine/threonine phosphatase PTC1. *Mol. Biol. Cell.* 9:917–930. http://dx.doi.org/10.1091/mbc.9.4.917

Rujano, M.A., F. Bosveld, F.A. Salomons, F. Dijk, M.A. van Waarde, J.J. van der Want, R.A. de Vos, E.R. Brunt, O.C. Sibon, and H.H. Kampinga. 2006. Polarised asymmetric inheritance of accumulated protein damage in higher eukaryotes. *PLoS Biol.* 4:e417. http://dx.doi.org/10.1371/journal.pbio.0040417

Schneider, C.A., W.S. Rasband, and K.W. Eliceiri. 2012. NIH Image to ImageJ: 25 years of image analysis. *Nat. Methods.* 9:671–675. http://dx.doi.org/10.1038/nmeth.2089

Scholz, D., J. Förtsch, S. Böckler, T. Klecker, and B. Westermann. 2013. Analyzing membrane dynamics with live cell fluorescence microscopy with a focus on yeast mitochondria. *Methods Mol. Biol.* 1033:275–283. http://dx.doi.org/10.1007/978-1-62703-487-6_17

Schott, D., J. Ho, D. Pruyne, and A. Bretscher. 1999. The COOH-terminal domain of Myo2p, a yeast myosin V, has a direct role in secretory vesicle targeting. *J. Cell Biol.* 147:791–808. http://dx.doi.org/10.1083/jcb.147.4.791

Sesaki, H., and R.E. Jensen. 1999. Division versus fusion: Dnm1p and Fzo1p antagonistically regulate mitochondrial shape. *J. Cell Biol.* 147:699–706. http://dx.doi.org/10.1083/jcb.147.4.699

Sesaki, H., and R.E. Jensen. 2001. *UGO1* encodes an outer membrane protein required for mitochondrial fusion. *J. Cell Biol.* 152:1123–1134. http://dx.doi.org/10.1083/jcb.152.6.1123

Sherman, F. 1991. Getting started with yeast. *Methods Enzymol.* 194:3–21. http://dx.doi.org/10.1016/0076-6879(91)94004-V

Sikorski, R.S., and P. Hieter. 1989. A system of shuttle vectors and yeast host strains designed for efficient manipulation of DNA in Saccharomyces cerevisiae. *Genetics.* 122:19–27.

Song, J., Q. Yang, J. Yang, L. Larsson, X. Hao, X. Zhu, S. Malmgren-Hill, M. Cvijovic, J. Fernandez-Rodriguez, J. Grantham, et al. 2014. Essential genetic interactors of *SIR2* required for spatial sequestration and asymmetrical inheritance of protein aggregates. *PLoS Genet.* 10:e1004539. http://dx.doi.org/10.1371/journal.pgen.1004539

Spokoini, R., O. Moldavski, Y. Nahmias, J.L. England, M. Schuldiner, and D. Kaganovich. 2012. Confinement to organelle-associated inclusion structures mediates asymmetric inheritance of aggregated protein in budding yeast. *Cell Reports.* 2:738–747. http://dx.doi.org/10.1016/j.celrep.2012.08.024

Swayne, T.C., C. Zhou, I.R. Boldogh, J.K. Charalel, J.R. McFaline-Figueroa, S. Thoms, C. Yang, G. Leung, J. McInnes, R. Erdmann, and L.A. Pon. 2011. Role for cER and Mmr1p in anchorage of mitochondria at sites of polarized surface growth in budding yeast. *Curr. Biol.* 21:1994–1999. http://dx.doi.org/10.1016/j.cub.2011.10.019

Tong, A., and C. Boone. 2007. High-throughput strain construction and systematic synthetic lethal screening in *Saccharomyces cerevisiae. Methods Microbiol.* 36:369–386. http://dx.doi.org/10.1016/S0580-9517(06)36016-3

Van Mullem, V., M. Wery, X. De Bolle, and J. Vandenhaute. 2003. Construction of a set of *Saccharomyces cerevisiae* vectors designed for recombinational cloning. *Yeast.* 20:739–746. http://dx.doi.org/10.1002/yea.999

Vowinckel, J., J. Hartl, R. Butler, and M. Ralser. 2015. MitoLoc: A method for the simultaneous quantification of mitochondrial network morphology and membrane potential in single cells. *Mitochondrion.* 24:77–86. http://dx.doi.org/10.1016/j.mito.2015.07.001

Wach, A., A. Brachat, C. Alberti-Segui, C. Rebischung, and P. Philippsen. 1997. Heterologous *HIS3* marker and GFP reporter modules for PCR-targeting in *Saccharomyces cerevisiae. Yeast.* 13:1065–1075. http://dx.doi.org/10.1002/(SICI)1097-0061(19970915)13:11<1065::AID-YEA159>3.0.CO;2-K

Wagih, O., M. Usaj, A. Baryshnikova, B. VanderSluis, E. Kuzmin, M. Costanzo, C.L. Myers, B.J. Andrews, C.M. Boone, and L. Parts. 2013. SGAtools: one-stop analysis and visualization of array-based genetic interaction

screens. *Nucleic Acids Res.* 41(W1):W591–W556. http://dx.doi.org/10.1093/nar/gkt400

Warren, G., and W. Wickner. 1996. Organelle inheritance. *Cell.* 84:395–400. http://dx.doi.org/10.1016/S0092-8674(00)81284-2

Westermann, B. 2014. Mitochondrial inheritance in yeast. *Biochim. Biophys. Acta.* 1837:1039–1046. http://dx.doi.org/10.1016/j.bbabio.2013.10.005

Westermann, B., and W. Neupert. 2000. Mitochondria-targeted green fluorescent proteins: convenient tools for the study of organelle biogenesis in *Saccharomyces cerevisiae. Yeast.* 16:1421–1427. http://dx.doi.org/10.1002/1097-0061(200011)16:15<1421::AID-YEA624>3.0.CO;2-U

Wong, E.D., J.A. Wagner, S.W. Gorsich, J.M. McCaffery, J.M. Shaw, and J. Nunnari. 2000. The dynamin-related GTPase, Mgm1p, is an intermembrane space protein required for maintenance of fusion competent mitochondria. *J. Cell Biol.* 151:341–352. http://dx.doi.org/10.1083/jcb.151.2.341

Youngman, M.J., A.E. Hobbs, S.M. Burgess, M. Srinivasan, and R.E. Jensen. 2004. Mmm2p, a mitochondrial outer membrane protein required for yeast mitochondrial shape and maintenance of mtDNA nucleoids. *J. Cell Biol.* 164:677–688. http://dx.doi.org/10.1083/jcb.200308012

Zhou, C., B.D. Slaughter, J.R. Unruh, A. Eldakak, B. Rubinstein, and R. Li. 2011. Motility and segregation of Hsp104-associated protein aggregates in budding yeast. *Cell.* 147:1186–1196. http://dx.doi.org/10.1016/j.cell.2011.11.002

Zhou, C., B.D. Slaughter, J.R. Unruh, F. Guo, Z. Yu, K. Mickey, A. Narkar, R.T. Ross, M. McClain, and R. Li. 2014. Organelle-based aggregation and retention of damaged proteins in asymmetrically dividing cells. *Cell.* 159:530–542. http://dx.doi.org/10.1016/j.cell.2014.09.026

Züchner, S., I.V. Mersiyanova, M. Muglia, N. Bissar-Tadmouri, J. Rochelle, E.L. Dadali, M. Zappia, E. Nelis, A. Patitucci, J. Senderek, et al. 2004. Mutations in the mitochondrial GTPase mitofusin 2 cause Charcot–Marie–Tooth neuropathy type 2A. *Nat. Genet.* 36:449–451. http://dx.doi.org/10.1038/ng1341